INTEGRATED MULTISCALE, NUMERICAL, EXPERIMENTAL, AND FIELD INVESTIGATION OF A LESS DAMAGING FRICTION REDUCER TO MITIGATE FORMATION DAMAGE IN UNCONVENTIONAL SHALE RESERVOIRS

A Dissertation

by

RIXING ZHANG

Submitted to the Office of Graduate and Professional Studies of
Texas A&M University
in partial fulfillment of the requirements for the degree of

DOCTOR OF PHILOSOPHY

Chair of Committee,	Nobuo Morita
Committee Members,	Hadi Nasrabadi
	Jerome Schubert
	Mahmoud El-Halwagi
Head of Department,	Jeff Spath

May 2021

Major Subject: Petroleum Engineering

ABSTRACT

Among the additives in slickwater fracturing, only friction reducers (FRs) are heavy molecular polymers, many of which are polyacrylamide-based. Although they are useful for their intended purpose, FRs rapidly decrease the production rate in shale by damaging the formation. Molecular dynamics simulation was used to evaluate how salts potentially encountered during fracturing treatments affect polyacrylamide-based FRs. This work focuses on evaluating the efficacy of a new, less-damaging FR using various methods such as core flood, UV-VIS, and precipitation tests. A field trial was also conducted, and the results show that this less-damaging FR can better mitigate formation damage compared with conventional FRs. Although production decline still occurs in a treated well, it is slower than that of a control well treated with a conventional FR.

The radius of gyration results from molecular dynamics simulations show the salt-tolerant patterns of PAM and HPAM follow a trend in which trivalent ions affect polymers more than bivalent ones, and monovalent ions affect the polymers the least. This result is consistent with results reported in the literature. This research predicts that the polymer chains in a less-damaging FR should be in the medium to short-range, the polymer concentration should be much lower, and nanoparticle fillers are necessary. The turbidities of the less-damaging FR solutions are almost ten times lower than those of HPAM. In addition, this new FR has only a negligible reaction with selected salts. Core flood test results indicate that the permeability lost via conventional FR is 92.6% to 99.8%. In contrast, the permeability damage via the less-damaging FR is 0.8%. In the field test, two wells on the same platform were treated with two different FRs. After three months of production, a comparative decline of gas production rate in measurable formation damaged by the less-damaging FR (10% reduction of initiated production rate) and a conventional inverse emulsion FR (30% reduction of daily gas production) was observed.

DEDICATION

This dissertation is dedicated to

My Beloved wife (Liping Deng), for her love and endless support, I wouldn't have finished my PhD without her.

My beloved parents (Yanjun Li and Jinbo Zhang) for their support and love.

My dear sons (Shiqi Zhang and Aiden Zhang), for their accompany and being good friends of mine.

ACKNOWLEDGEMENTS

I would like to thank my previous committee chair academic advisor, Dr. Nasr-El-Din, who passed away during my research. I appreciate my current committee chair academic advisor, Dr. Nobuo Morita. I am grateful for his continuous encouragement, guidance, and support during the last year for my research. I appreciate his help on devoting his invaluable time to review my research work and evaluate its results and to give advice. I hope to extend my appreciation to my committee members, Dr. Nasrabadi, Dr. Schubert, and Dr. El-Halwagi, for their guidance and support throughout the course of my research.

Thanks also go to student members, lab technicians, and administrative officers of Dr. Nasr-El-Din group and Dr. Morita group. Many thanks also to my friends and colleagues and the department faculty and staff for making my time at Texas A&M University a great experience.

Finally, thanks to my wife, my parents, my sons, for their encouragement, patience, and love to me.

CONTRIBUTORS AND FUNDING SOURCES

Contributors

This work was supervised by a dissertation committee consisting of Professor Nobuo Morita [advisor] and Hadi Nasrabadi and Jerome J. Schubert of the Department of [Home Department] and Professor Mahmoud M. El-Halwagi of the Department of [Outside Department].

All work conducted for the dissertation was completed by the student independently.

Funding Sources

Graduate study was supported by a fellowship from Texas A&M University.

NOMENCLATURE

FR – Friction Reducer

EUR – Estimated Ultimate Recovery

SRV – Simulated Reservoir Volume

TOC – Total Organic Content

EOR – Enhanced Oil Recovery

LDFR – Less Damaging Friction Reducer

HPAM – Partially hydrolyzed Polyacrylamide

ACS – American Chemical Society

HPHT – High Pressure High Temperature

UV-VIS – Ultraviolet Visible

PAM – Polyacrylamide

TABLE OF CONTENTS

Page

LIST OF FIGURES

LIST OF TABLES

Page

CHAPTER I

INTRODUCTION

Oil and gas have been produced economically from shale plays by combining the horizontal drilling and hydraulic fracturing, ushering in a revolution in the shale oil and gas industry. However, the production of oil and gas from shale has declined rapidly over the past few years. This is due to the formation damage caused during slickwater fracturing treatments of shale reservoirs.

It is well known that slickwater is the most commonly used fracturing fluid system. However, this method may actually cause low EUR and rapid production decline. Among the chemicals used in slickwater, only the friction reducer (FR) is a long chain, high molecular weight polymer such as polyacrylamide. All other slickwater components are of such small molecular weight that they cannot be considerable factors in formation damage.

Slickwater treatments do perform generally well, barring any external effects, such as encountering metal ions during the treatment procedure. However, in shale formations, there are several metal ions (Ca^{2+}, Mg^{2+}, etc.) present in the formation water. Furthermore, during fracturing, pad acid can react with the metal tubulars and produce Fe^{3+} as a result. This iron precipitation is not only very damaging to shale formations, but also causes FR precipitation. Some biocides also degrade the performance of slickwater fracturing treatments. Researchers have studied formation damage caused by

FRs in different ways; however, no systematic multiscale research has to date been conducted.

Development and Refinement of Multistage Hydraulic Fracturing Technologies

The deep-rooted concept of developing unconventional oil resources is that "the larger the SRV, the higher the production rate and EUR" because Mitchell Energy proved for the first time that unconventional shale oil and gas resources could be efficiently developed by combining slick water fracturing with horizontal drilling in Barnett Shale in1997. The more slick-water pumped, the more shale volume to be fractured, and more gas to be produced (Texans, 2016). The slick water is pumped to the formation at high pumping rate to break the hard shale rock. The water leak-off to the shale formation from the fracture faces triggers the slip of the pre-existing natural fractures at critical status and form a fractured network, which is called SRV (Zoback, 2010).

The development and refinement of the disruptive technology called "High Volume Multistage Hydraulic fracturing of Long Horizontal Well with Slick Water" originated from Barnett shale. It has established the commercial development of shale plays around the world. Based on the fundamental research on shale from Nanoscale to reservoir scale and field experiences, lessons learned from different shale plays, some industry protocols to develop unconventional oil and gas reservoirs are summarized below:

(1) Screening sweet spots by integrating total organic content (TOC) in shale, Fracability Index (consider both brittleness and fracture toughness), and

natural fracture density, in-situ stress contrast, etc. (Walton and McLennan, 2013, Jin et al., 2015, Sonnenberg, 2015, Portas and Slatt, 2016, Slatt et al., 2016);

(2) Drilling longer laterals and fracturing more stages with dense perforations to increase the surface area to the pay zones (King, 2010, Mayerhofer et al., 2010, Smith and Montgomery, 2015);

(3) Conduct hydraulic fracturing surveillances like micro seismic and tracer technologies to monitor hydraulic fracturing process, inter-well interference, inter-fracture interference, interactions between induced and natural fractures, flowback and production profile, etc. (Warpinski et al., 2009, King, 2012, Goswick and LaRue, 2014, Maxwell, 2014).

(4) Implement downhole Isolation equipment (degradable or non-degradable) and degradable chemical diverters for maximizing the SRV (Lindsay et al., 2016, Weddle et al., 2017).

(5) Implement slick water system for hydraulic fracturing and adapt the system with different viscosities and pumping rates for reservoirs of different natural fracture density and in-situ stresses, so that a relatively desirable SRV can be generated (Dusseault and McLennan, 2011, Vermylen and Zoback, 2011, Zoback et al., 2012, Hofmann et al., 2014).

(6) Use highly efficient clean friction reducers and relatively high pumping rate to fracture the shale formation and increase the propped surface area (Wu, 2010, Lindsay et al., 2011).

To develop unconventional resources more efficiently, the operator must adapt the mechanical tools and slick water system to the specific reservoir conditions. A general slick water system composition for the US shale plays is plotted in Figure 1 with source data from the FracFocus database (www.fracfocus.org) maintained by the National Hydraulic Fracturing Chemical Registry. The chemical additives depicted on the smaller pie represent less than 0.8% of the total fluid volume. Generally, the concentration of the additives in most slick water systems is a relatively consistent 0.5% to 2% with water making up 98% to 99.2% for different subsurface conditions. The number of chemical additives used in a fracturing treatment varies case by case. Selection depends on the specific conditions of the subject well, such as geology characteristics of the shale formation, water chemistry, downhole temperature, completion design, and so on. A typical stimulation usually uses very low concentrations of 3 to 12 additive chemicals. The commercial development of unconventional oil and gas resources is mainly attributed to the merit of the slick water to create a complex permeable fracture network without using highly-pressured water. But every coin has two sides, the low EUR and high production decline rate might be also attributed to the interactions between shale rock and slick water system (Barati et al., 2011, Banerjee et al., 2017).

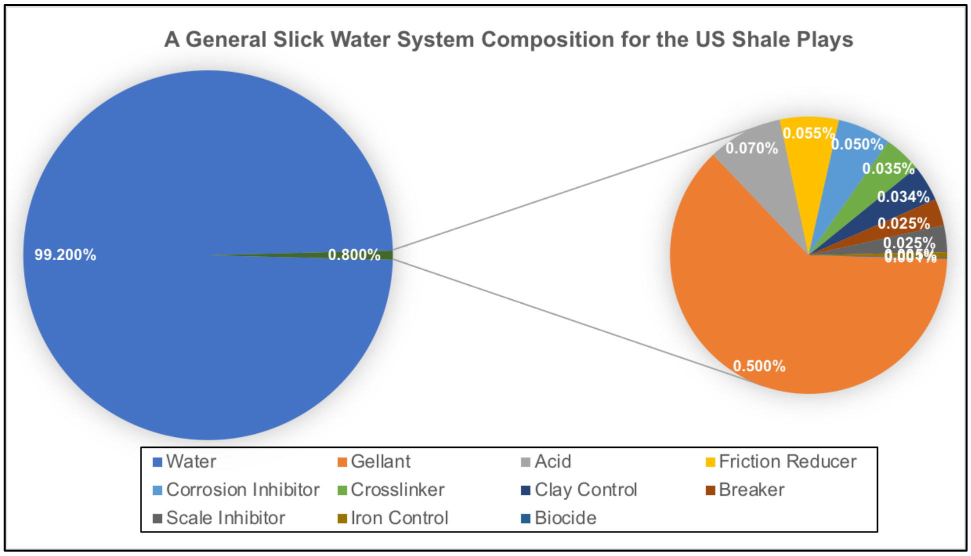

Figure 1: Volumetric Composition of a General Slick Water System for the US Shale Plays (edited with source data from www.fracfocus.org)

Unconventional Shale EOR Potential and Challenges in the U.S.

Learning from the successful experience of developing unconventional shale gas in the past decades, advanced drilling and completion technologies like extended-lateral horizontal drilling and massive multistage hydraulic fracturing have been successfully leveraged in the development of unconventional shale oil reservoirs. Progressive and significant production enhancements have been achieved in US unconventional oil plays, e.g. Permian Basin, Eagle Ford, Bakken Shale, Oklahoma Stack & Scoop, DJ Basin, etc. The Energy Information Administration (EIA) estimates that the U.S. daily production rate of unconventional oil has been increased significantly from 0.8 MMBOPD (16.5% of total U.S. daily oil production) in 2008 to 5.6 MMBOPD (56.5% of total U.S. daily oil production) in 2018 (EIA, 2019). The unconventional oil production from the existing and emerging plays will continue playing a vital role through 2050 because EIA projected that the total U.S. unconventional shale oil daily production rate will increase gradually to about 7.9 MMBOPD (70.1% of the total U.S. daily oil production) by 2050 (EIA, 2019). It is observed that the unconventional industry has been pursuing maximum stimulated reservoir volume (SRV) by drilling longer horizontal wells and fracturing as manageable stages as possible, adding as much proppant as possible, etc. (King, 2010, Mayerhofer et al., 2010). A record 17,935 feet (3.4 miles) lateral length with 100% in the zone of Wolfcamp Shale, Permian Basin was achieved in April 2019 (Veazey, 2019). Although breakthroughs in drilling and completion of unconventional oil wells have been achieved, the full potential of the U.S. unconventional oil has yet to be realized, and the recovery factors of most shale oil wells in the liquid-rich plays are less than 10%, which is much lower than conventional reservoirs (Panja et al., 2016, Panja and Deo, 2016). The incremental production rates of unconventional oil plays do not increase proportionally to the increase of lateral length, number of stages, proppant loading, etc., and the production decline rates do not get lower either (Joshi, 1991, Cipolla and Wallace, 2014, Gubian, 2017). Besides, the return of investment does not increase with increasing cost either. It is estimated that every one percent increase in unconventional oil recovery factor could add 10 to 25 billion barrels of oil to the U.S. technically recoverable oil resource base (EIA, 2019). According to data from our laboratory experiments and field pilots, and the statistics of the number of vertical and horizontal wells in five major unconventional oil plays, conservative estimate is that the depleted fractured vertical wells can recover additional 2,100 bbls oil from one Huff-N-Puff treatment (estimated based on Figure 11). The depleted fractured horizontal wells can recover additional 25,000 bbls oil from one Huff-N-Puff treatment (estimated based on Figure 13). The total EOR potential of the existing wells in the five major US shale oil plays is 549 MM bbls oil. The EOR potential of each play is calculated and shown in Table 1. If the Huff-N-Puff treatment is repeated several times, more additional oil might be recovered. Therefore, the current technologies to unlock the potential of unconventional oil reservoirs and enhance oil recovery is the bottleneck. It is important to investigate the fundamental reasons for production decline curve of unconventional oil wells as related to the tight rock matrix interactions with the fracturing fluids.

Table 1: ***EOR Potential of the Major Unconventional Oil Plays in the U.S.***

Play Name	Number of Vertical Wells	Number of Horizontal Wells	EOR Potential (MM bbls)
Permian Basin	30,378	6,039	215
Eagle Ford	0	14,973	374
DJ Basin	8,046	7,815	212
Bakken	0	11,358	284
SCOOP/STACK	0	2,535	63
TOTAL	38,424	42,747	1,148

The Structure of Shale

The pore-size distribution of shales is mainly small, down to several nanometers. Relatively large pores with poor connections can be up to four microns. Pores can also be connected by thin conduits down to 15 nanometers (Figure 2) (Sisk et al. 2010; Kuila and Prasad 2011). If big polymers are injected to the formation flocculate, the pore throats most likely would be plugged.

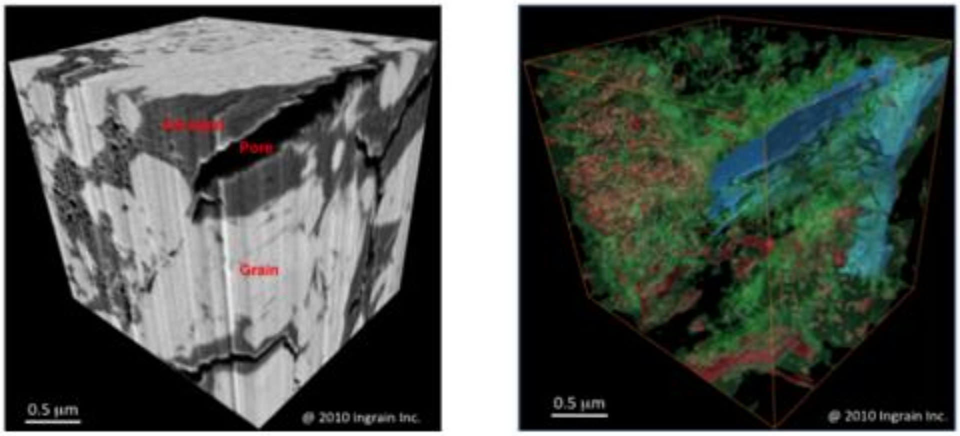

(a) (b)

Figure 2: (a) Rendered volume of shale at the highest nano-resolution. (b) Kerogen (green), disconnected pores (red) and connected porosity (blue). The scale is 500 nanometers

Slickwater fracturing was developed and used in other unconventional reservoirs, such as tight gas sand and shale (Carman and Cawiezel 2007). The evolution of fracturing fluids has alternated between oil-based, water-based, and liquefied natural gas fracturing fluids (Barati and Liang 2014). Because the FRs primarily used for slickwater fracturing are polyacrylamides, which are synthetic polymers, the perception was that they would be difficult to break.

Slickwater Fracturing Fluids

In slickwater fracturing fluid, water, and proppant occupy 99% of the fluid-system volume (Jackson et al. 2011). Other additives like acid, FRs, surfactant, potassium chloride, scale inhibitor, pH adjusting agent, iron control agents, corrosion inhibitors, and biocides are also added to fracturing fluid at low concentrations to fulfil different purposes for different fracturing jobs (Figure 3).

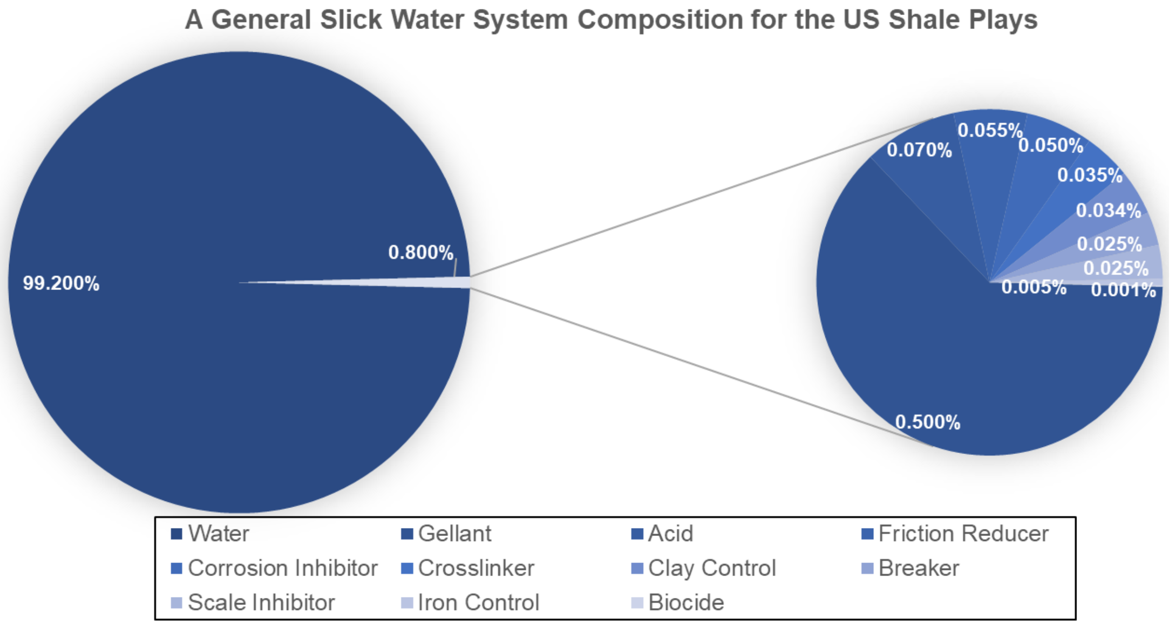

Figure 3: Volumetric composition of a general slickwater system for the US shale plays (edited with source data from www.fracfocus.org)

Typical Treatment Procedure of Slickwater Fracking

The typical slickwater-fracturing treatment typically includes the following steps as shown in Table 2.

Table 2: Different stages of slickwater fracturing (Holloway and Rudd 2013)

NO.	Pumping Steps of	Fluid Injected in Each Stage	Function

	Slickwater Fracturing		
1	An acid stage	Several thousand gallons of water mixed with a dilute acid such as hydrochloric or muriatic acid	This serves to clear cement debris in the wellbore and provide an open conduit for other frac fluids by dissolving carbonate minerals and opening fractures near the wellbore.
2	A pad stage	Approximately 100,000 gallons of slickwater without proppant material	The slickwater pad stage fills the wellbore with the slickwater solution (described below), opens the formation and helps to facilitate the flow and placement of proppant material.
3	A prop sequence stage	May consist of several substages of water combined with proppant material (consisting of a fine mesh sand or ceramic material, intended to keep open, or "prop" the fractures created and/or enhanced during the fracturing operation after the pressure is reduced)	This stage may collectively use several hundred thousand gallons of water. Proppant material may vary from a finer particle size to a coarser particle size throughout this sequence.
4	A flushing stage	A volume of fresh water sufficient	Flush the excess proppant from the wellbore

Potential Formation Damage during Slickwater Fracturing

While friction reducers (FRs) are essential to any slickwater fracturing fluid system in shale, many chemical components present in the formation can cause interact with the FR and cause formation damage **(**Figure 4**)**. The other elements in Figure 4 include Zn, Ba, Cu, and Mn elements. Si is excluded from the acid reaction results (Peña-Icart et al., 2011; Tessier et al., 1979). Although the majority of the previous research focused on evaluating the friction-reducing performance of these chemicals, only a few studies have addressed the potential formation damage (Ibrahim et al. 2018).

Several metal ions are generated and dissolved in fracturing fluid and flowback fluid. In the whole procedure, the FR is in a kind of brine environment. Polyacrylamide-based FRs will precipitate when they meet with different salts in water. The sizes of PAM/HPAM polymers are larger than most formation pores but smaller than fracture size. Without metal ions, the formation damage caused by FRs may not be that severe. However, in the presence of metal ions the HPAM FRs coil or precipitate, making their sizes are much bigger, and resulting in serious formation damage. In addition, breaking these polymers at temperatures lower than 200°F remains challenging (Woodroof and Anderson 1977).

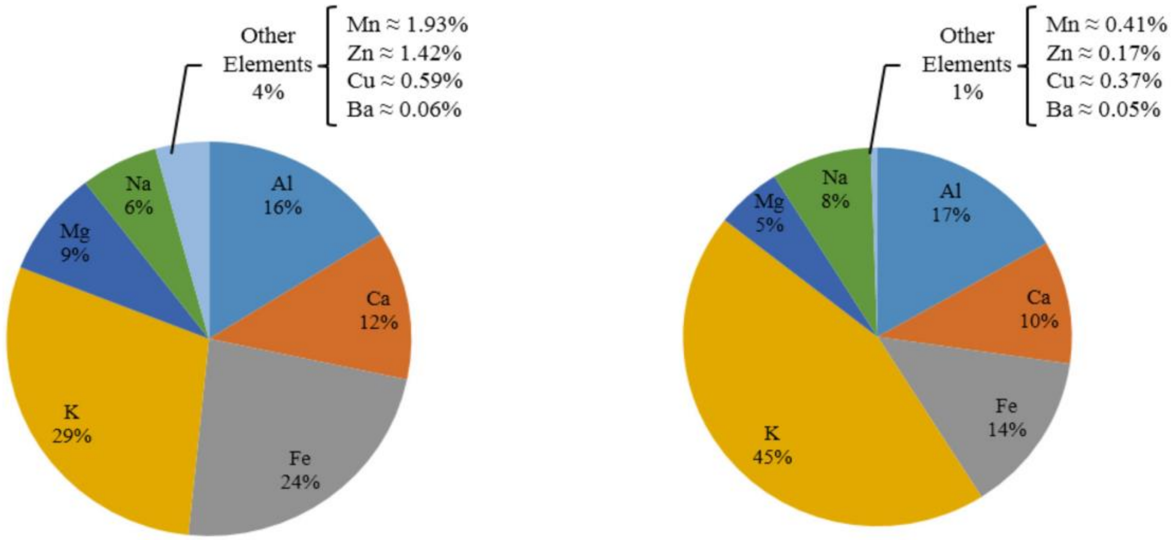

(a) (b)

Figure 4: The six major elements of the (a) Otter Park and (b) Evie shale samples obtained by acid digestion

The pay zones of unconventional oil and gas formations exhibit these intrinsic properties: relatively high content of clay and TOC (total organic content), pore volumes at the scale of nanometer, permeability at the scale of Nano Darcy, and relatively high natural fracture density. Clay exhibits the highest ratio of surface area to volume compared against other minerals in unconventional formation. Higher the ratio of surface area to volume, stronger is the absorption ability of mineral (Banerjee et al., 2017). Partially hydrolyzed polyacrylamide (HPAM) is the main component of slick water. The typical molecular weight of HPAM is at the scale of several million g/mole. The typical size of HPAM is at the scale of microns, which is three orders of magnitude of shale pore volume. Besides, HPAM is very sensitive to the brine salinity and hardness, especially in contact with Ca^{2+}, Mg^{2+}, Fe^{3+} in the formation, and may cause damage to the formation, as is shown in Figure 5 and Figure 6 (Wu et al., 2017). The dynamic adsorption process was studied in the laboratory at microscale with SEM and NMR, as shown in Figures 4 and 5 (Guo et al., 2018). Gellant is another common high molecular weight polymer being commonly used in hydraulic fracturing to carry proppant. The size of most gellants is also at the scale of microns. Although gellant breakers are used commonly in the field, not all gellants can be cracked and the residuals can also affect fracture conductivity (Montgomery, 2013). Therefore, it is important to understand the fundamental mechanisms governing the damage of slick water system to the fracture network, so that feasible approaches can be developed to increase the Estimated Ultimate Recovery (EUR) of unconventional resources (Pancharoen, 2009).

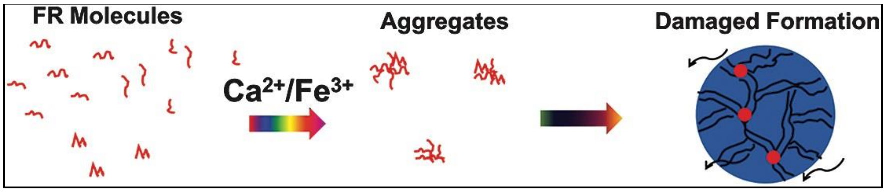

Figure 5: Formation Damage Caused by the Flocculation of Friction Reducer Molecules (Wu et al., 2017)

Figure 6: Effect of Fe^{3+}on the Flocculation of Friction Reducer Molecules (Wu et al., 2017). Fe^{3+} is from the common mineral pyrite in the shale formation.

For a typical hydraulic fracturing fluid job in the US, tens of millions of gallons of base fluid are pumped containing fracturing fluid additives at a concentration less than 1% (as shown in Figure 1). The injected fluid leaks-off into the fractured shale formation and allows a filter cake to be formed on the fracture face. In the low-permeability shale formations, the gellants tend to form thick filter cake on the fracture surface, which can adversely affect the fracture conductivity. The low viscosity system in shale fracturing tends to create narrower fracture width. Furthermore, the proppant concentration in massive shale fracturing is much lower than that of conventional fracturing due to the relatively lower viscosity fluid system employed for the purpose of creating complex fracture network. Due to the low proppant concentration, the effects of gel residue to the fracture network may be magnified (Smith and Montgomery, 2015). Because of the permanent nature of the metallic cross-linker, the molecular weight of the broken gel residue is much greater than that formed from linear gels. This also causes a greater degree of proppant pack damage and conductivity loss, as shown in Figure 9 (Smith and Montgomery, 2015). Field observations indicate that only 15-30% of the fracturing water is recovered during the flowback (Alkouh et al., 2013). However, the large amount of fracturing fluid additives left in the fracture network might cause contamination to the propped fractures, fracture surfaces, shale matrix, and natural fractures, as are demonstrated in Figure 10. In summary, the outcome of the contamination to the stimulated reservoir volume are: (1) the reduction of permeability on & near the fracture surfaces, (2) the loss of conductivity in major fractures; (3) the blockage of pores and natural fractures near the fracture surfaces; (4) the decrease of effective fracture length and height; (5) extra pressure drop across the near fracture surface areas and in the propped fractures (Barati et al., 2011); and ultimately, (6) impairing the post-frac production, accelerating production decline rate and relatively lower EUR. The contaminations are attributed to the fundamental structure and composite of unconventional shale rock and chemicals in the slick water system are permanent unless remediated properly.

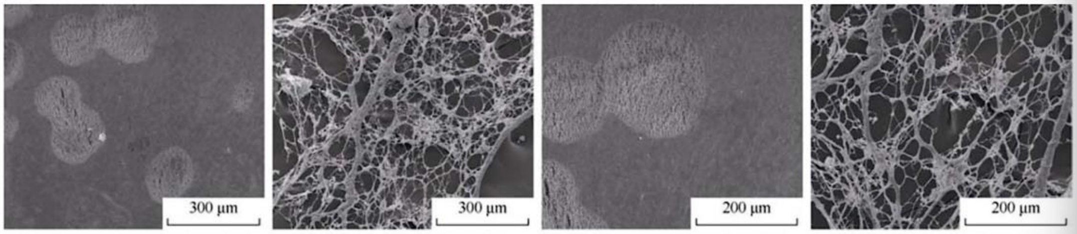

(a) Blank sample before adsorption, 300 times (b) The sample after adsorption, 300 times (c) Blank sample before adsorption, 500 times (d) The sample after adsorption, 500 times

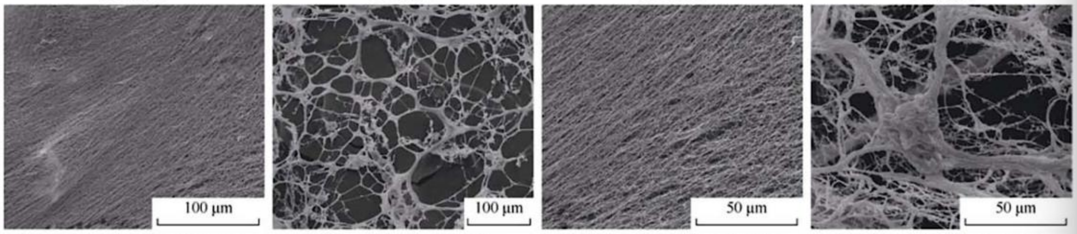

(e) Blank sample before adsorption, 1 000 times (f) The sample after adsorption, 1 000 times (g) Blank sample before adsorption, 2 000 times (h) The sample after adsorption, 2 000 times

Figure 7: SEM Images of Before & After Adsorption on Shale Surfaces at Different Resolutions (Guo et al., 2018)

Sequence number	Time	Sagittal plane 1	Sagittal plane 2	Sagittal plane 3
1	20 min	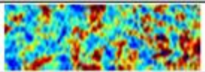	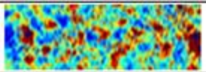	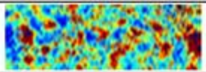
2	60 min	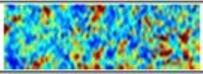	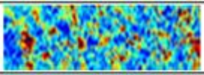	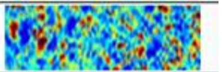
3	150 min	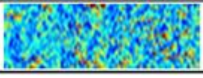	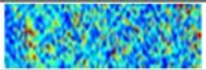	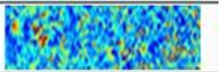

Figure 8: NMR Images Showing Dynamic Adsorption Process of HPAM on Shale Surfaces on Three Sagittal Planes (Guo et al., 2018). The red color represents pores, the blue color represents HPAM, the dimension of the sample is 1 inch in diameter and 3 inch in length.

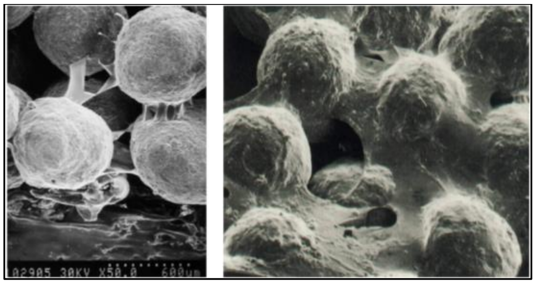

Figure 9: Proppant Pack Damage Caused by Gellants (Smith and Montgomery, 2015). If not being remediated properly, these gellants will stay in the proppant pack for decades.

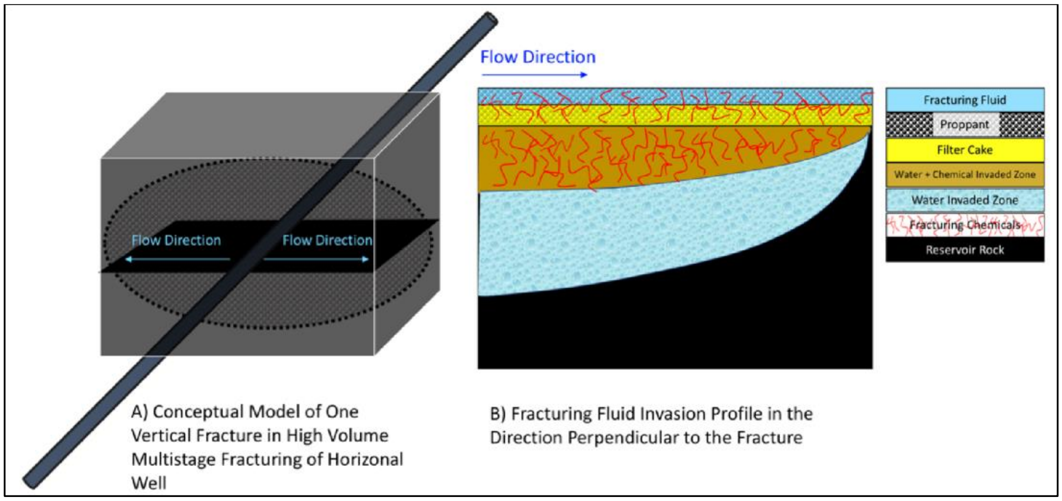

Figure 10: Interactions between the Slick Water System and Rock Matrix near the Fracture Surfaces

Metal Ions in Flowback

In flowback, different ions may affect friciton reducers (Montgomery 2013) or other long-chain polymers pumped into reservoirs (Table 3). PAM and HPAM polymers are unstable when temperature increases. PAM-based FR can precipitate in the presence of divalent and trivalent cations, resulting in formation damage (Seright et al. 2009).

Therefore, cations in flowback water should be considered carefully to prevent the FR from precipatating.

Table 3: The surface charge density of the focus ions (Essington 2005)

Ion	Charge(C)	Ion Radius (pm)	Surface Area (m^2)	Surface Charge Density(C/m^2)
Na^+	1.60E-19	116	1.69E-19	0.9462
K^+	1.60E-19	152	2.90E-19	0.5511
Ca_2^+	3.20E-19	114	1.63E-19	1.9594
Ba_2^+	3.20E-19	149	2.79E-19	1.147
Cl^-	-1.60E-19	167	3.50E-19	-0.4565
SO_4^{2-}	-3.20E-19	290	1.06E-19	-0.3028

$FeCl_3$ After Acid Flush

In fracturing treatments, among other chemicals, hydrochloric acid is largely used to dissolve minerals and initiate cracks in a formation. During the operation, the acid readily dissolves rust in the tubing or casing and corrodes steel equipment where it is mixed and pumped through. The acid also attacks iron-containing minerals in a formation under treatment. Iron could also be presented in dissolved or suspended form in produced water. When the fracturing fluid mixes with subsurface water and reacts with carbonate rocks and shale, the pH increases as the acid/fracturing fluid is consumed, and the dissolved iron starts to precipitate in the form of gelatinous iron hydroxide unless an effective iron control system is applied. The insoluble iron precipitation may accumulate in the reservoir and near the wellbore, thereby plugging or reducing the created and natural permeability of the reservoir. Dill and Smolarchuk (1988) have indicated that the above phenomenon, i.e., precipitation of iron in natural and newly developed fractures, is one of the main causes of formation damage. The iron can also precipitate and form scale within the tubing, which also reduces production.

The dissolved trivalent ferric ions react with polyacrylamide and flocculate in water (Kaşgöz et al. 2003). Water treatments always use this mechanism to remove tervalent ferric ions from water. But this reaction will damage the formation and decrease the friction-reduction rate during slickwater fracturing.

CHAPTER II

MATERIALS

Chemicals

Partially hydrolyzed polyacrylamide (HPAM) was prepared by diluting a concentrated liquid obtained from a service company and had a molecular weight of 12 million. The Less-Damaging Friction Reducer (LDFR) used was obtained from another service company in liquid form. This LDFR was composed of several short chain polymers and surfactants and like HPAM, was diluted from a concentrated solution before testing.

The salts used for this work include NaCl, $CaCl_2$, $MgCl_2$, and $FeCl_3$ as these cations are commonly found in the formation. ACS grade versions of each salt of 99% purity were obtained from various vendors and weighed before being added directly to the polymer solution for testing.

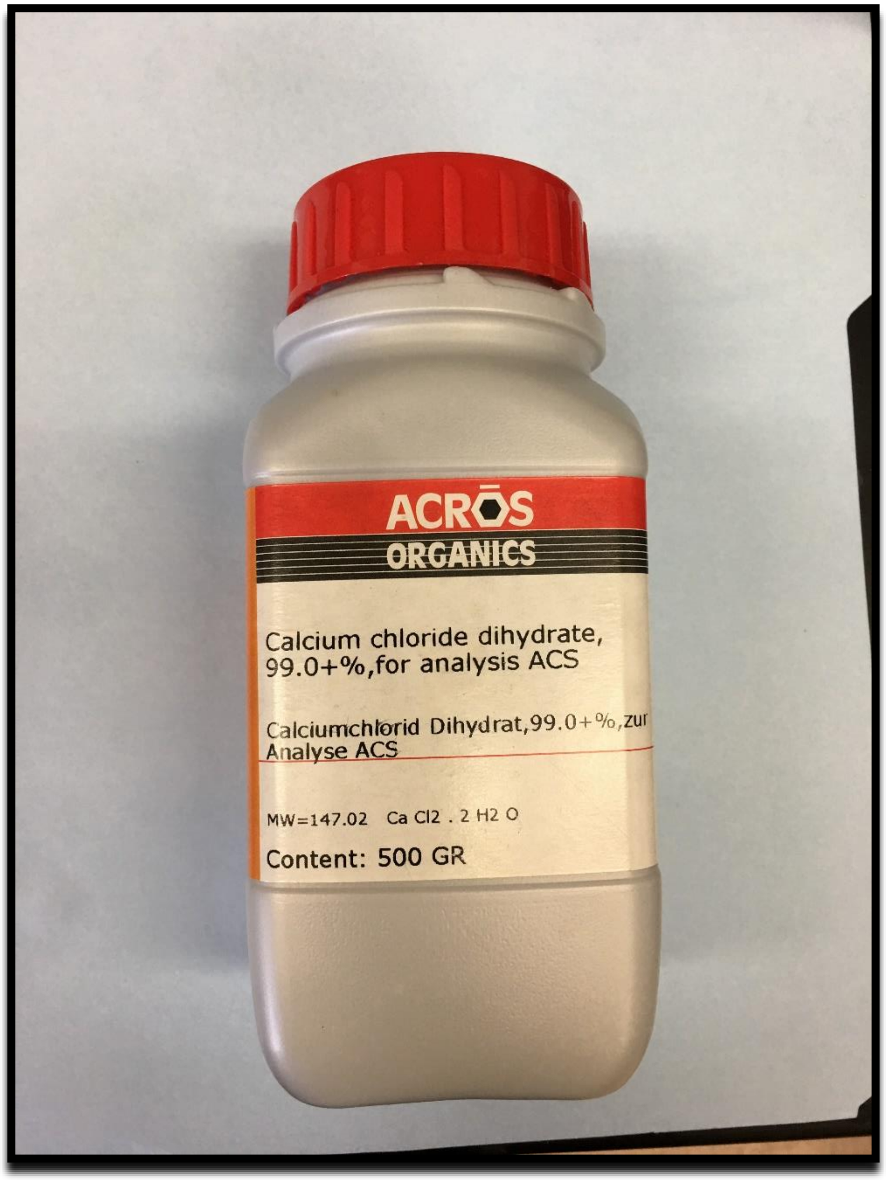

Figure 11: Bottle of $CaCl_2 \cdot 2H_2O$ used for testing.

HCl was used in order to dissolve some of the precipitate formed during the testing process. 8 wt.% HCl solution was obtained from LaMotte as shown in Figure 12 and was added directly to the precipitate.

Figure 12: HCl solution used to dissolve precipitates.

Cores

Carbon Tan

6” length Carbon Tan Sandstone cores were obtained from Kocurek Industries for core flood experiments. These cores were selected due to their permeability range common for hydraulic fracturing treatments. The properties of the core can be found in Table 4. Images of the cores used can be seen in Figure 13.

Table 4: Carbon Tan core data for core flood.

Items	Value
Material	Sandstone
Dimensions (L x D)	6” x 1.5”
Porosity	13%
Permeability	8.3-18.71 mD

Figure 13: Carbon Tan cores used for core flood as obtained.

The mineralogical details of the Carbon Tan cores can be found in Figure 14 below. This composition was obtained through XRD (X-ray powder diffraction).

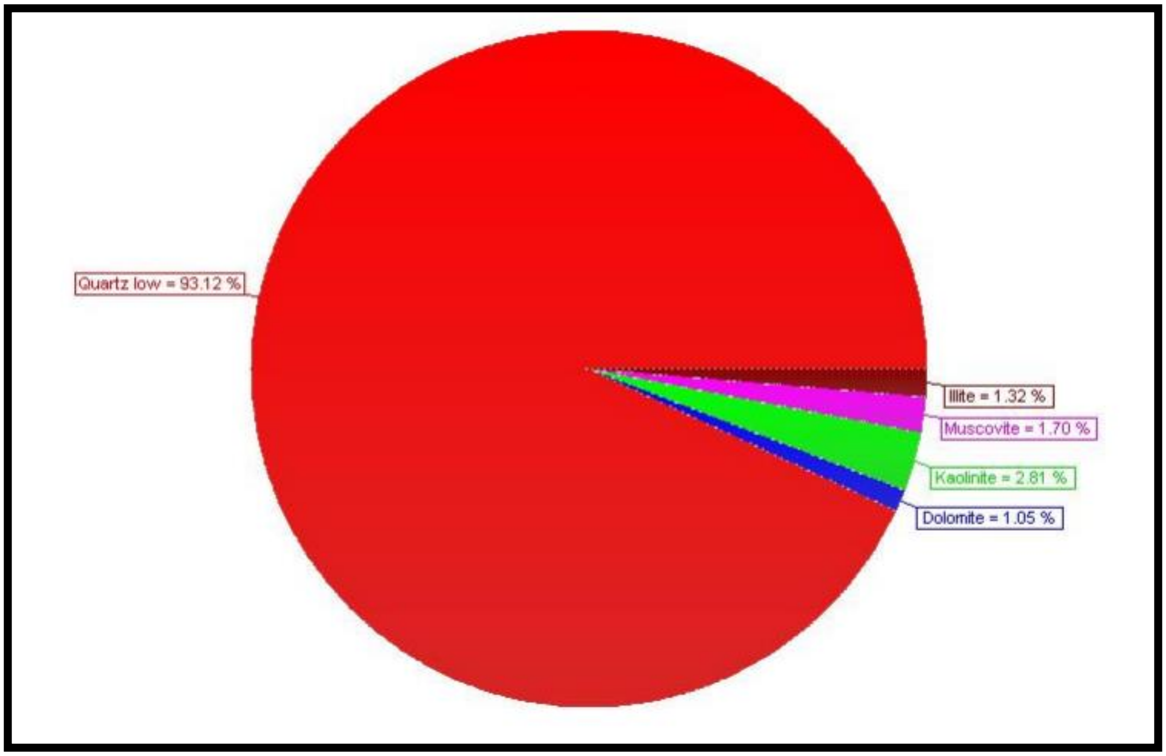

Figure 14: Mineral composition of Carbon Tan cores.

Proppant

Cores made from synthetic quartz proppant were prepared by packing a hollow stainless-steel core with synthetic quartz. Before placing the synthetic quartz into the core, the cores were first washed and dried to remove any dust or dirt. One end of the metallic core was then sealed and taped shut using a 120-mesh stainless steel fiber filtration cloth and duct tape. Next, the synthetic quartz was carefully added into the dried core up to the brim of the cylinder as shown in Figure 15.

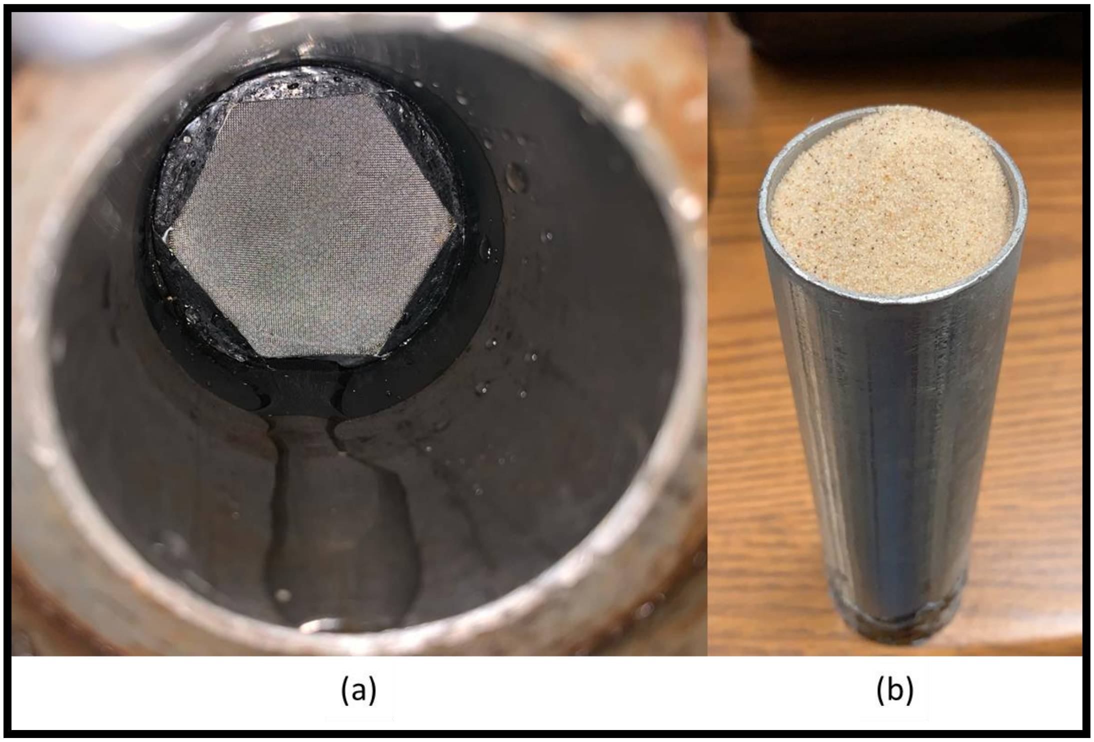

Figure 15: (a) Washed empty hollow metallic core. (b) Hollow metallic core packed with synthetic quartz.

Once the core was filled, another piece of steel mesh was placed over the opening and securely duct taped into place to prevent any of the synthetic quartz from falling out. The final appearance of the stainless-steel core can be seen in Figure 16. Six such cores were created using a variety of synthetic quartz and similarly packed as shown in Figure 17. The proppant sizes used were 20/40 mesh, 40/70 mesh and 100 mesh.

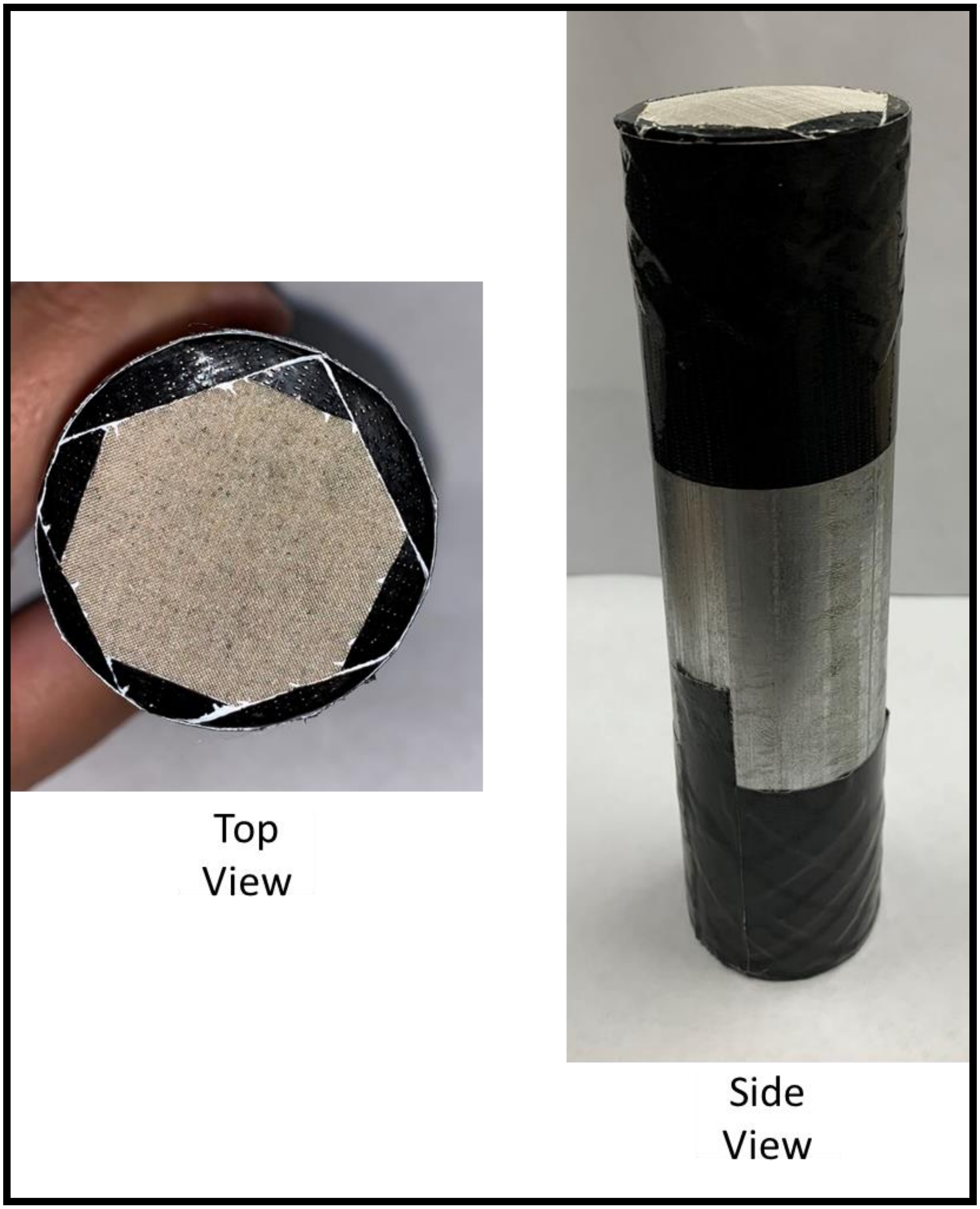

Figure 16: Top and side view of completed synthetic quartz core after it has been properly packed.

Figure 17: Synthetic quartz cores to be tested.

CHAPTER III

EQUIPMENT

Core flood

The core flood setup is shown in Figure 4. Two 2L piston accumulators were used to store an 8 wt.% KCl brine and the FR solution to be tested which were displaced using a piston accumulator. Valves are installed at the inlets and outlets of each accumulator to control fluid switching during the injection process. A pressure transducer was used to measure the pressure drop across the core and this data was recorded on a nearby computer.

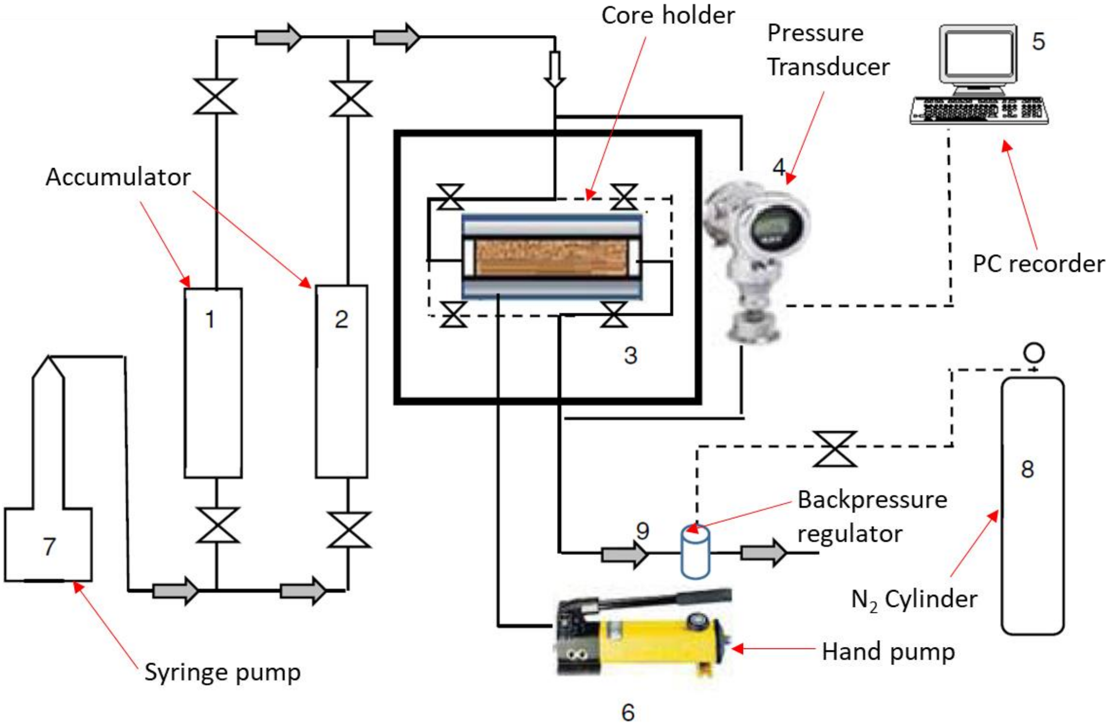

Figure 18: Core flood setup used.

Valves were also installed at the inlet and outlet of the core holder in order to control the flow direction through the core. A backpressure regulator connected to a N_2

cylinder was connected to the core outlet in order to maintain a backpressure of 500 psi. A hand pump was used to apply overburden pressure on the core during injection. This pressure was set at 300 psi above the injection pressure.

Viscometer

Viscosity measurements for this experiment were carried out with 2 viscometers. One of them was a Grace M5600 HPHT viscometer shown in Figure 19. This tabletop viscometer had a maximum pressure limit of 2000 psi and a max temperature limit of 500°F. A B5 bob attachment constructed out of Hastelloy was used to measure the viscosity of the polymer solutions. 50 ml of polymer solution was added to a Hastelloy cup before being attached to the viscometer. The temperature of the cup was controlled using an oil bath attachment that would be raised to cover the cup during the experiment.

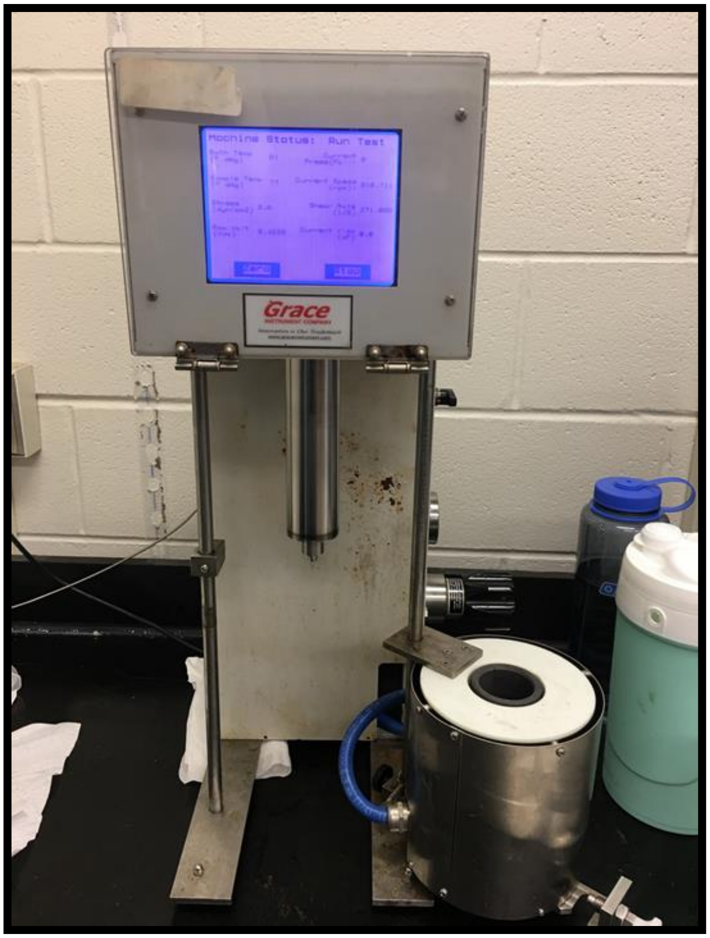

Figure 19: Grace M5600 Viscometer used for viscosity testing.

The other viscometer used was a RheoSense m-VROC micro viscometer. This viscometer requires a minimum of 50 µl of solution per test and has a maximum temperature capability of 158°F. The required volume of polymer was loaded into the syringe which was subsequently locked in place and covered with the thermal jacket.

Figure 20: RheoSense m-VROC viscometer.

UV-VIS Spectrophotometer

The UV-VIS experiments were carried out using a Thermo Scientific GENESYS^{TM} 10 UV-VIS Spectrophotometer. These tests were carried out at room temperature and pressure, and at a wavelength of 600 nm. A 1 cm x 1 cm cuvette containing the solution was inserted into the viscometer to be measured. The transmittance of the solution was allowed to stabilize before being recorded.

CHAPTER IV

PROCEDURE

Experiments

Polymer Preparation

500 ml each of 1.5 wt.% HPAM and LDFR solution was prepared in a Waring blender shown in Figure 21 below. First, 500 ml of DI water was added to the blender and the shear rate was increased in order to form a vortex. Next, 7.5 g of powdered HPAM or LDFR were added to the side of the vortex slowly in order to allow for proper hydration and to prevent the formation of fish eyes. As the solution thickened, the shear rate was increased to maintain the vortex for even mixing. After adding all the solid, the mixture was allowed to stir for a further 15 minutes to ensure complete hydration of the additives. A properly hydrated solution is shown in Figure 22. These polymer solutions were used for core flood, precipitation, and viscosity tests. For the latter two tests, salts were added and further mixed after the 15 minutes of mixing.

Figure 21: Waring blender used to prepare HPAM and LDFR solutions

Figure 22: Hydrated HPAM or LDFR solution to be used

Viscosity Measurements

Viscosity measurements using the Grace M5600 Viscometer required 50 ml of polymer solution to be added to the Hastelloy cup before being attached to the viscometer. The viscosity of the polymer was measured as a function of shear rate from

271 to 813 s^{-1}. These tests were carried out at room temperature and atmospheric pressure.

With the RheoSense m-VROC viscometer, viscosity measurements were carried out at much higher shear rates as a reflection of pumping rates during slickwater fracture treatments in the field. For HPAM, the viscosity measurements were carried out from 270.9 to 2573.5 s^{-1} shear rate. For LDFR, the shear rate was set from 270.9 to 4740.7 s^{-1}. The viscosity measurements were carried out at room temperature and atmospheric pressure. All viscosity points were recorded and then plotted against the shear rate.

Core flood

For each experiment, the KCl brine was first injected at a rate of 0.5 cm^3/min in a direction imitating flow from the reservoir to the wellbore. After the pressure across the core stabilized, 15 gal/1000 gal of FR solution was injected at a 0.5 cm^3/min in the same direction. Once the injection of FR solution was completed, the system was shut down for 12 hours before a second stage of KCl brine was injected. This second stage was injected at a rate of 0.5 cm^3/min and was done in order to investigate any formation damage caused by the FR.

UV-VIS

A Thermo Scientific GENESYS^{TM} 10 spectrophotometer was used to measure the transmittance of the sample solution. After each solution was prepared, it was added to a 1 cm x 1 cm cuvette before being placed in the spectrophotometer. The sides of the cuvette were wiped down with a kimwipe to remove any dust or debris before the reading was taken. The wavelength of the spectrophotometer was set to 600 nm for each test. Before operating the spectrophotometer, it was first calibrated by inserting a cuvette containing DI water.

Simulation

Molecular Dynamics Simulation was used to determine the behavior of PAM and HPAM during the slickwater fracturing process. The main simulation steps included amorphous cells installation, forcite geometry optimization, NPT (NPT means the condition of constant particle number N, constant pressure P, and constant temperature T), NVT (NVT means the condition of constant particle number N, constant volume V, and constant temperature T), forcite analysis, and comparison of results and variables optimization.

The radius of gyration (R_g) was used to quantify the conformation alteration of polymer chains. The smaller the R_g, the more coiled the polymer chain is. Such coiling is a result of the interactions between the metal ions present in the solution and heavily coiled PAM/HPAM chains lose their friction reducing properties and tend to flocculate. The radius of gyration, R_g, is defined as the root mean square distance of the atoms in the molecule from their common center of mass as shown in **Eq. 1**,

$$R_g = \sqrt{(\sum_{i=1}^{N} m_i s_i^2)/(\sum_{i=1}^{N} m_i)}, \ldots\ldots\ldots\ldots\ldots\ldots\ldots\ldots..(1)$$

where m_i represents the mass of the atom, s_i indicates the position of atom with respect to the center of mass of the molecule, and N is the total number of atoms.

Material Studio 2017R2 software was used to simulate molecular dynamics of PAM-based FRs in different salt solutions. For PAM amorphous cells, one 20-repeat units PAM, 5200 H_2O molecules, and a variety of metal cations (Ca^{2+}, Mg^{2+}, Fe^{2+} or Fe^{3+}) with the corresponding counter ion, Cl^- constituted a 53.8×53.8×53.8 Å (1 angstrom (Å) = 1×10^{-10} meters (m) = 0.1 nanometer (nm)) cube. Smart algorithm, COMPASS force field, 298K temperature, and 20ps simulation time were chosen.

CHAPTER V

FRICTION REDUCER SIMULATIONS

Simulation of PAM

The simulated structure of PAM with 20 repeating units is shown in Figure 23. In this figure, the red, blue, grey, and white dots represent oxygen, nitrogen, carbon, and hydrogen atoms respectively.

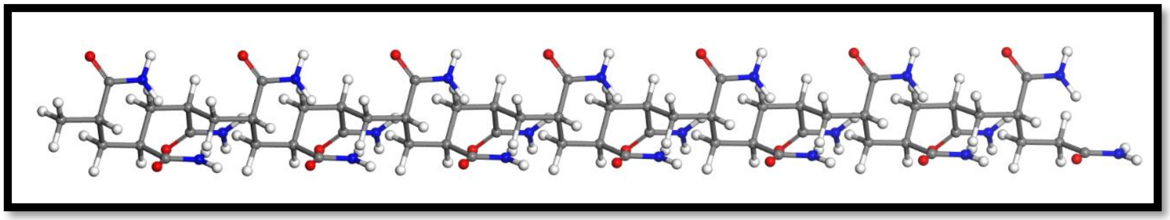

Figure 23: Non-ionic PAM with 20 repeated units

With this model of PAM, ferrous chloride solution was added to the model. The simulation results are shown in Figure 24 below. The initial conformation of the polymer can be seen on the left, where the polymer appears to be straight and uncoiled. However, after 20ps simulation, it can be observed that the polymer conformation had changed as a result of the influence from the ferrous ions present.

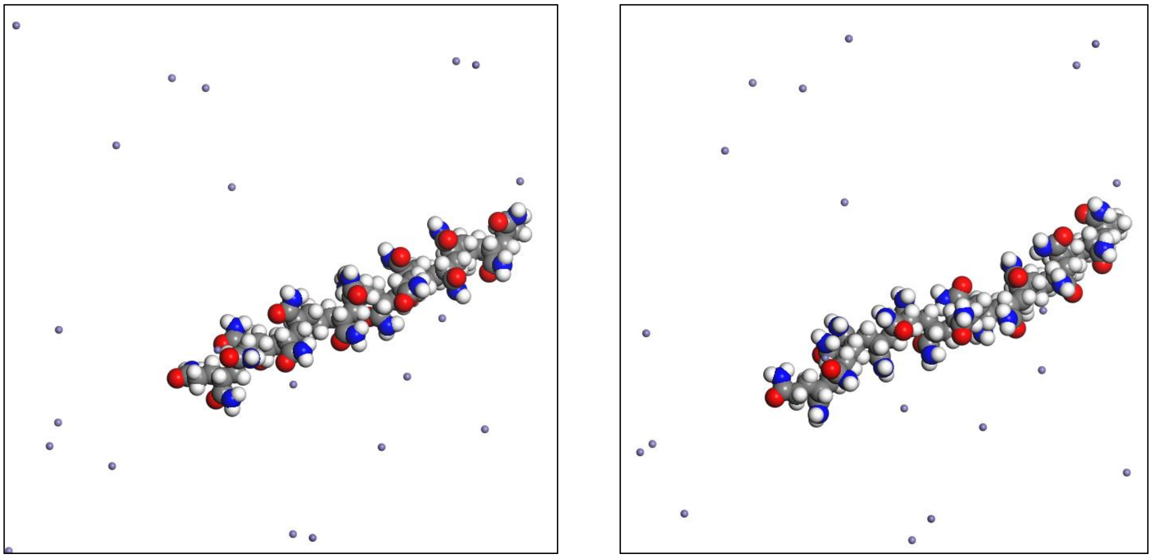

Figure 24: **PAM polymer's 3D configuration alteration before NVT beginning (left) and after 20ps simulation (right). Purple dots around the 20-unit PAM molecule represent Fe^{2+}.**

The radius of gyration was then evaluated in the presence of 4 different salts, $FeCl_3$, $CaCl_2$, $MgCl_2$, and $FeCl_2$. These salts were selected as they are commonly found in formation water. The concentrations of each salt were varied from 0 to 3 mol/L. The radius of gyration was then plotted as a function of concentration in Figure 25. From the results, it can be seen that PAM coils in all studied solutions. Furthermore, calcium ions were observed to affect PAM-based solutions less than magnesium, but more than ferrous ions. Ferric ions had the greatest effect on PAM coiling. As the concentration of the salt increases, the radius of gyration for PAM decreases indicating more coiling of PAM. This trend matches field experience where PAM FRs are known to lose more friction-reduction capability in the presence of ferric ions than with calcium ions.

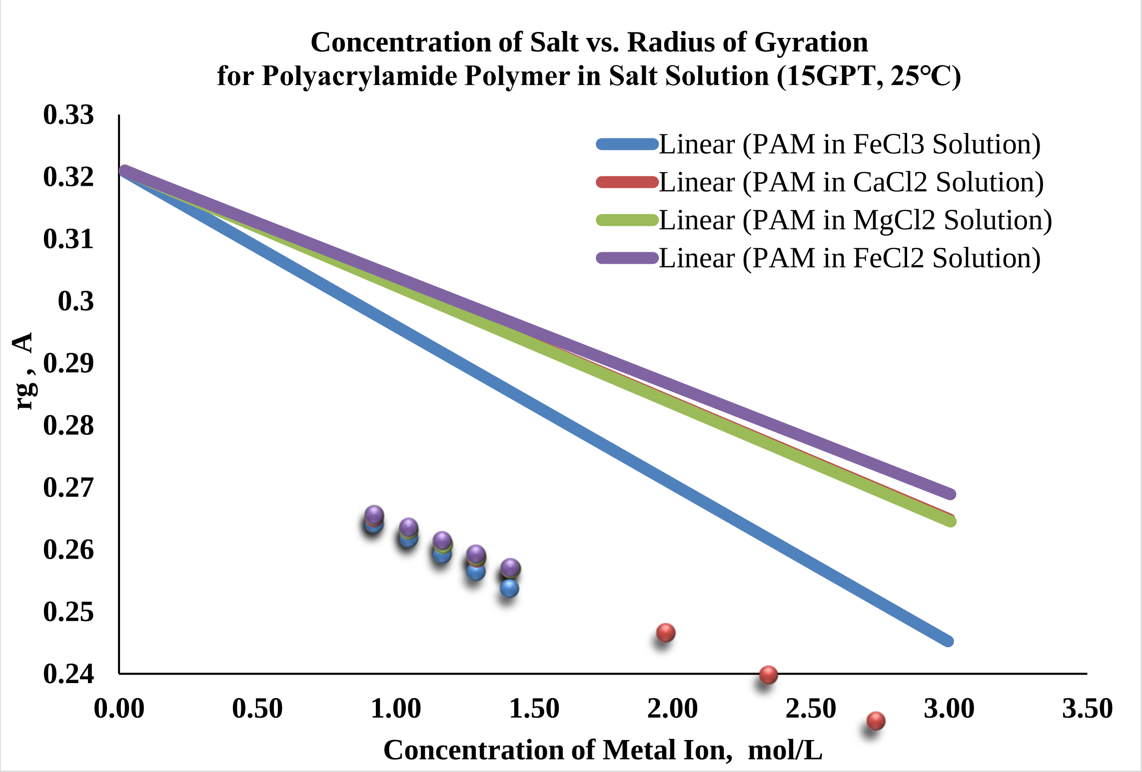

Figure 25: Change in radius of gyration when PAM interacts with different metal ions in different concentration.

Simulation of HPAM

HPAM (Partially Hydrolyzed Polyacylamide) is one of the most common FR available. It is made by reacting sodium acrylate with acrylamide so that approximately 30% of the acrylamide groups are in the hydrolyzed form with the structure shown in Figure 26.

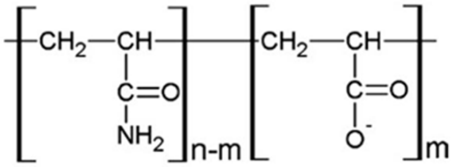

Figure 26: Repeating monomer units of HPAM

This hydrolyzed form improves the solubility in water, and makes the polymer more compatible with cations, and is commonly marketed as a 50% active dispersion in mineral oil. Because it is widely used as a flocculant for water in paper manufacture and the cheapest FR, it is the most widely used in the fracturing treatment (Montgomery 2013).

In this simulation, HPAM with 4 repeating units was used as shown in Figure 27. Just like in Figure 23, atoms are represented by red, blue, grey, and white dots corresponding to oxygen, nitrogen, carbon, and hydrogen atoms.

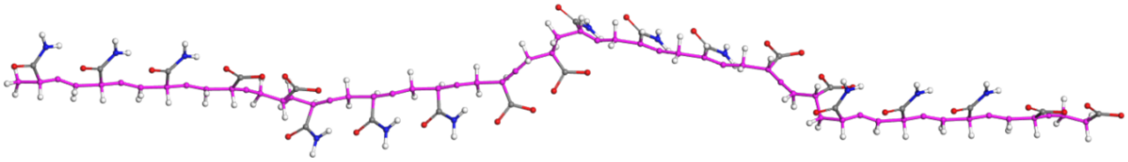

Figure 27: HPAM polymer with 4-repeat units

The simulation of the radius of gyration of HPAM was carried out with several mono-, di-, and trivalent ions such as NaCl, KCl, $FeCl_2$, $MgCl_2$, $CaCl_2$, and $FeCl_3$. The effect of these ions on the radius of gyration are shown in Figure 28.

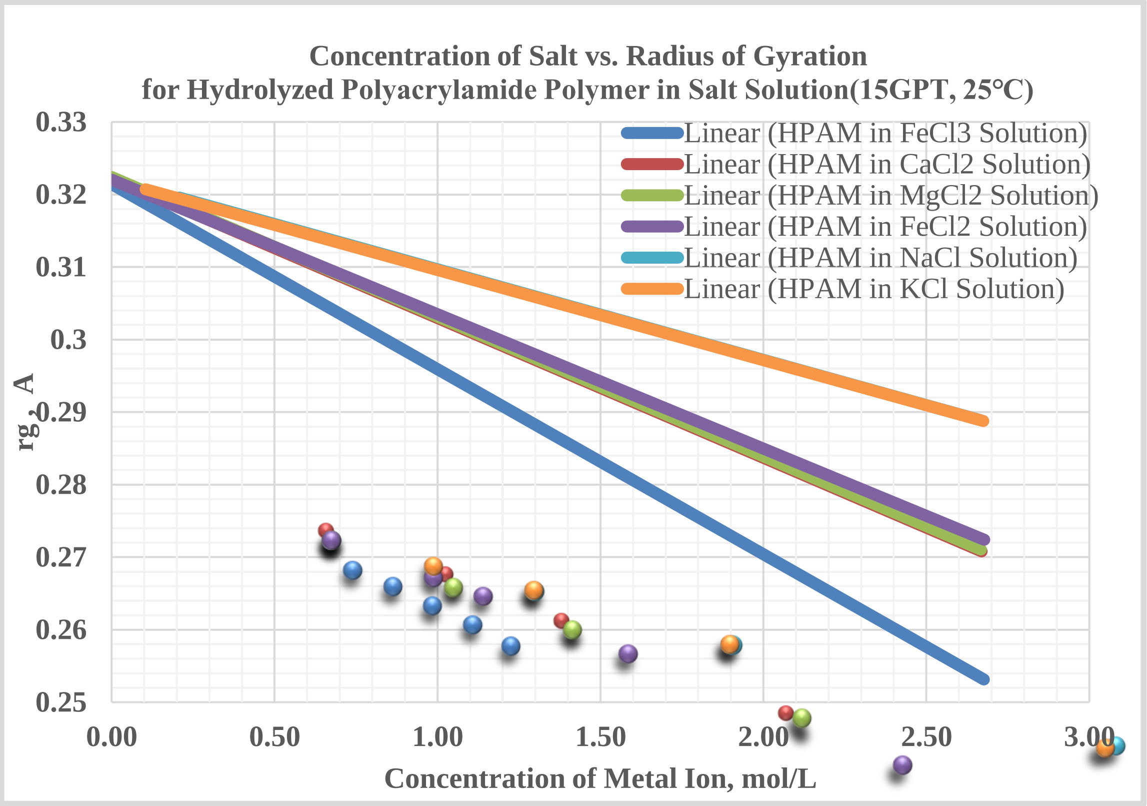

Figure 28: Radius of gyration evolution when HPAM interacts with different metal ions in different concentration

The radius of gyration of HPAM was shown to be affected by all cations tested. Like PAM, trivalent ions were shown to have a larger impact on the radius of gyration than mono- or divalent cations.

Effect of time on simulations

The effect of time on the simulation results of PAM and HPAM with metal ions was examined at 20ps and 200ps. This is necessary to determine if significant changes in ion-polymer interactions were present at longer periods of simulation time and therefore, if a longer simulation time was required. The simulation was repeated at 200ps using $FeCl_3$,

$MgCl_2$, and $CaCl_2$. The results were then plotted against those obtained at 20ps. Comparing 20ps with 200ps simulation time, the radius of gyration results was found to be similar. This indicates that a simulation time of 20ps is sufficient for all PAM and HPAM simulations (Figure 29 through Figure 31).

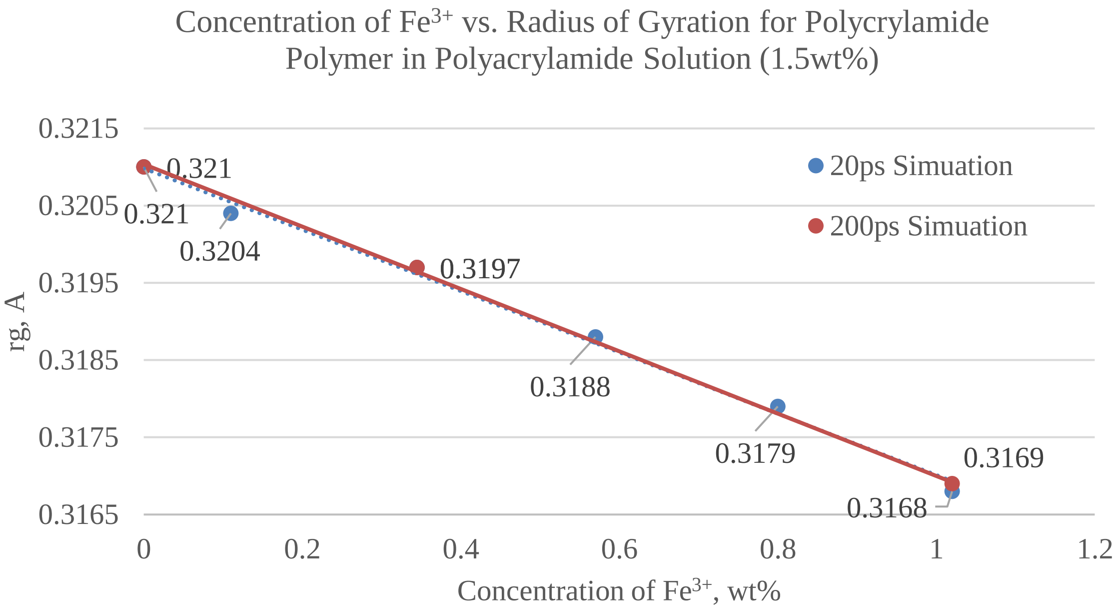

Figure 29: 20ps MD simulations vs. 200ps MD simulations in ferric chloride solutions ($1ps=10^{-12}$ s)

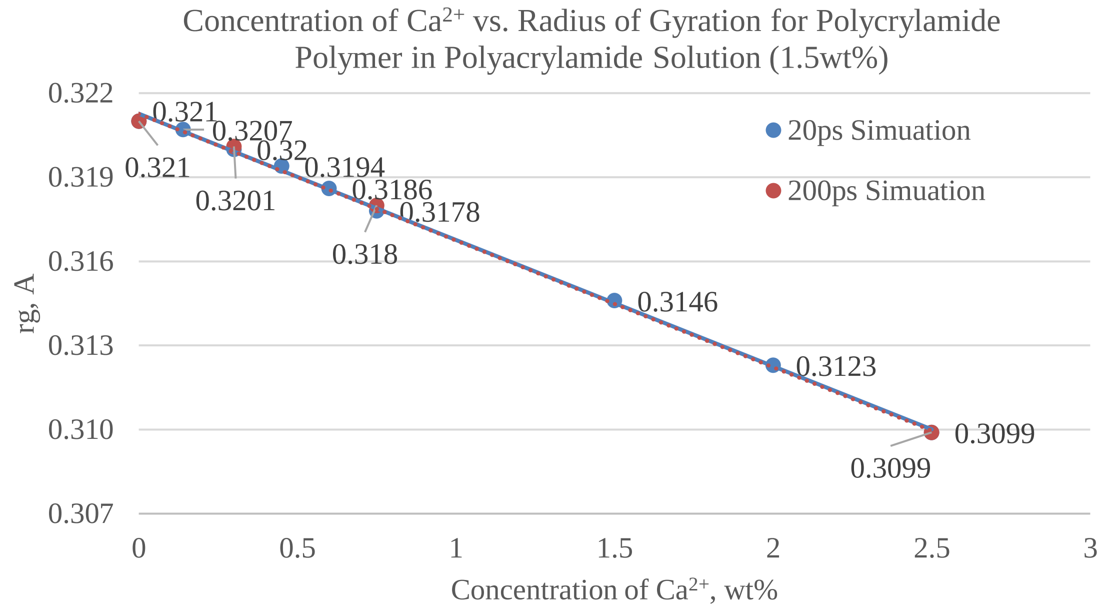

Figure 30: **20 ps MD simulations vs. 200ps MD simulations in calcium chloride solutions**

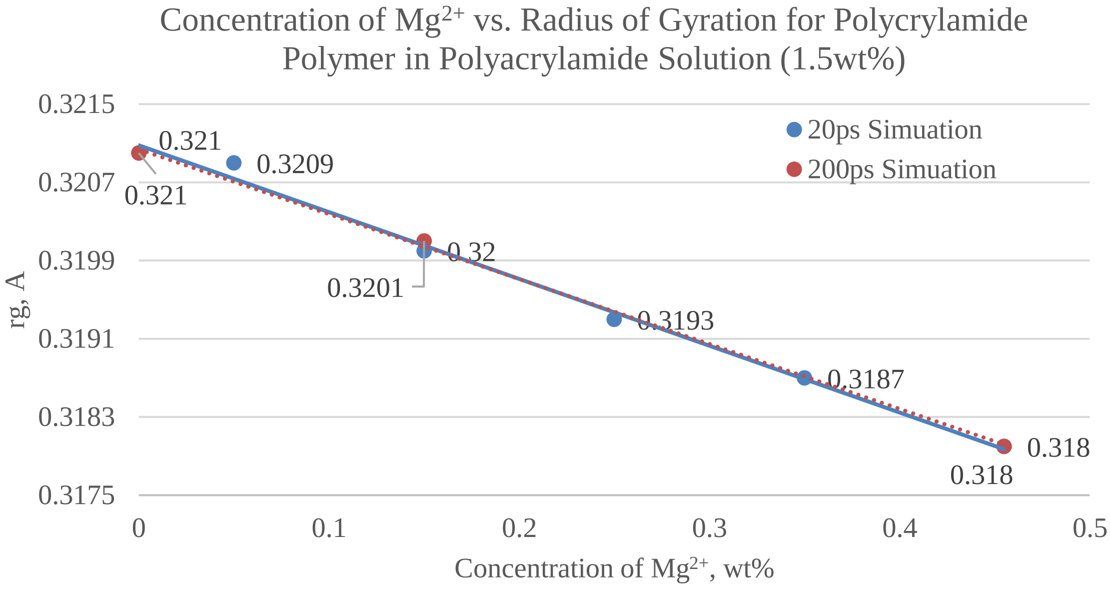

Figure 31: **20ps MD simulations vs. 200ps MD simulations in magnesium chloride solutions**

CHAPTER VI

EFFECT OF METAL IONS

Before any fracturing fluid solution is used, it is extremely important to verify the interactions of ions with the polymers or surfactants used. This is due to the extensive documentation of negative interactions of cations with these fracturing fluids that can cause loss of viscosity or crosslinking capability, reduced proppant carrying capacity, loss of friction reduction properties, and in severe cases, outright precipitation of the polymer or surfactant. This precipitation causes formation damage and the loss of fluid functionality results in failure of the hydraulic fracturing treatment as the remaining fluid is unable to fracture the rock.

Precipitation Tests

One of the common methods of evaluating interactions between the fracturing fluid and cations is through simply mixing them and observing the resulting mixture. 150 ml solutions of LDFR were prepared in 250 ml conical flasks and 5 wt.% of NaCl, $MgCl_2$, $CaCl_2$, and $FeCl_3$ were added. These flasks are shown in Figure 32.

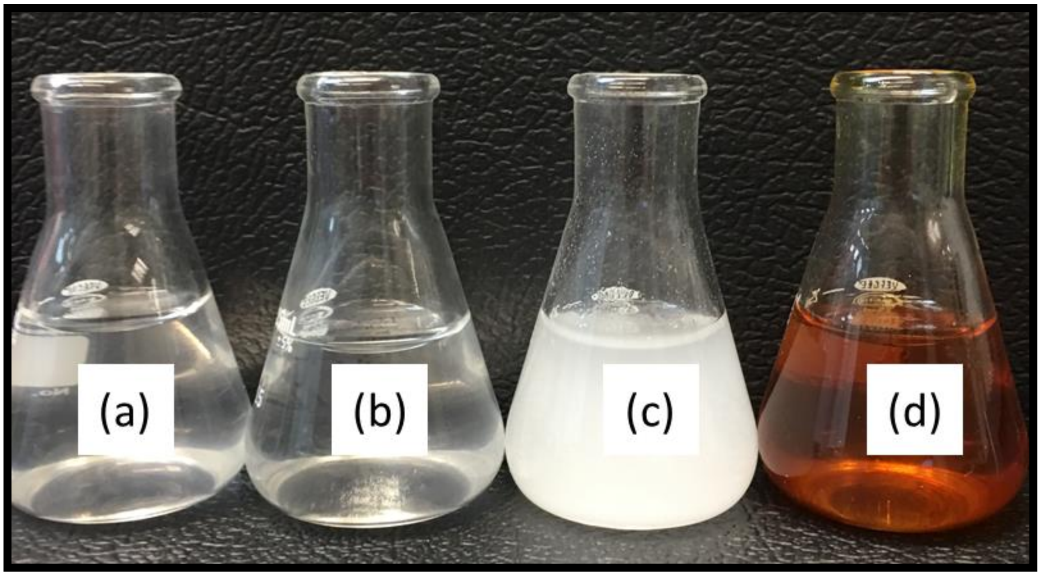

Figure 32: LDFR solutions with (a) NaCl, (b) MgCl2, (c) CaCl2, and (d) $FeCl_3$.

As can be seen from these tests, the Na^+, Mg^{2+}, and Fe^{3+} ions did not cause precipitation with the LDFR solution. However, the Ca^{2+} ions were observed to cause some precipitation with the LDFR. Since the pH of the LDFR solution is >9, it is likely that the precipitate formed is $Ca(OH)_2$. To determine if the precipitate was $Ca(OH)_2$ or LDFR fragments, HCl was added to the conical flask. Reducing the pH of the solution would dissolve any $Ca(OH)_2$ while if the precipitate was LDFR, it would not dissolve. The before and after images of flask (c) can be observed in Figure 33. After adding and mixing HCl, the white precipitate dissolves and the solution becomes clear. Therefore the precipitate must have been $Ca(OH)_2$. The overall lack of precipitation of the LDFR indicates that the LDFR has no negative interactions with these salts.

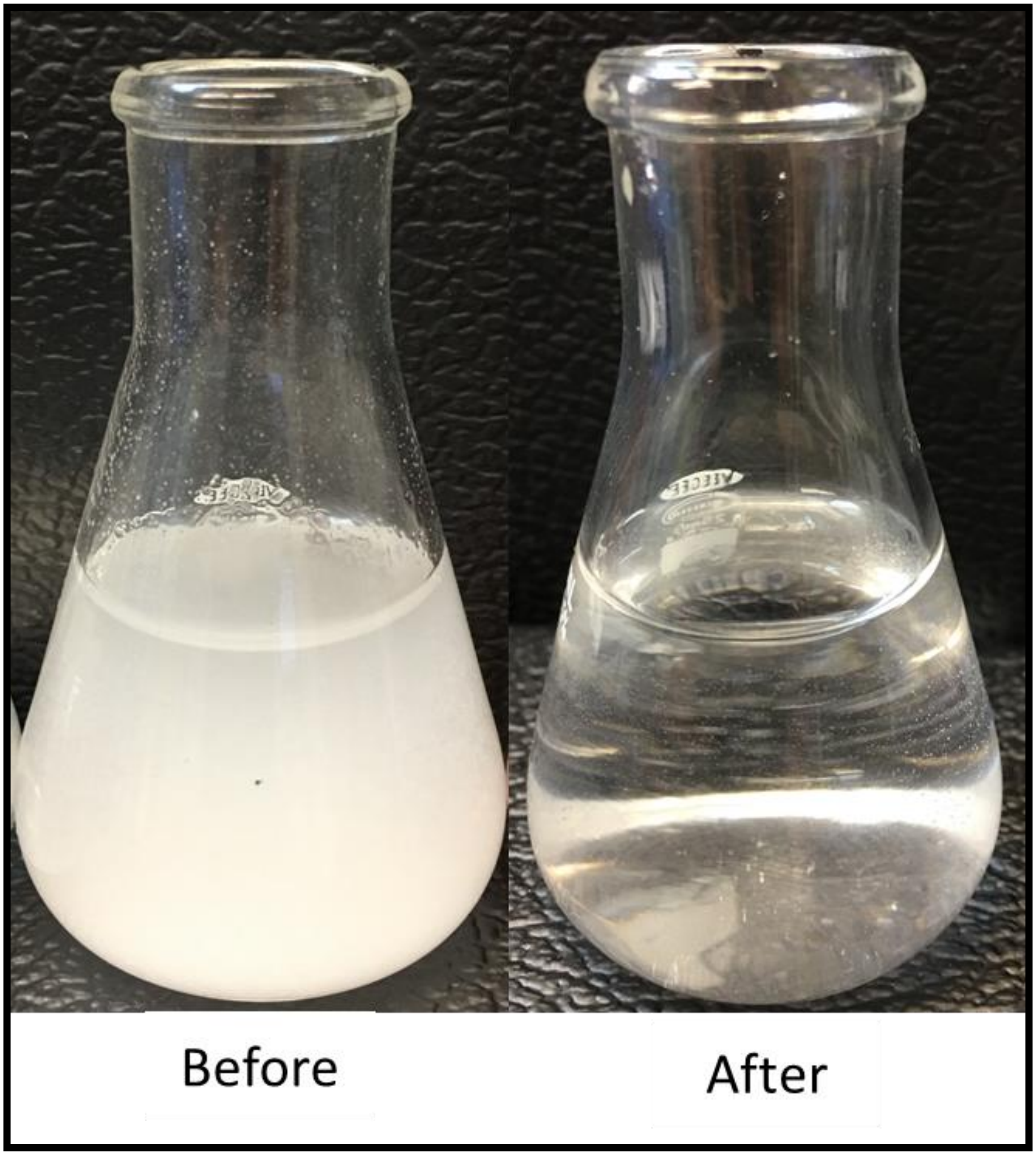

Figure 33: Before and after images of adding HCl to the mixture containing $CaCl_2$.

Next, the same tests were carried out with 1.5 wt.% HPAM solution. The same concentration of salt was dissolved in each HPAM solution. After mixing, the solutions were allowed to stand.

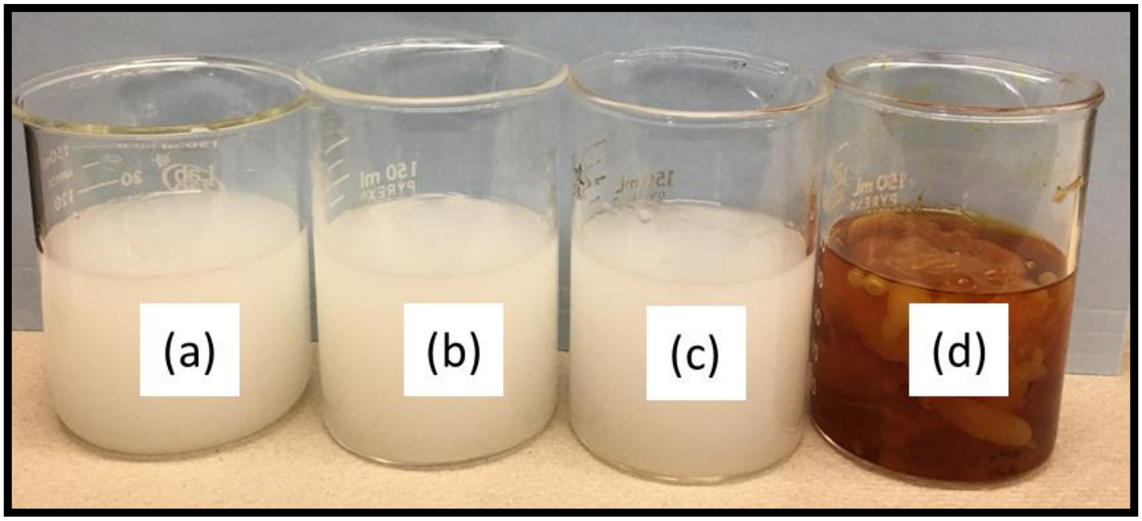

Figure 34: HPAM solutions with (a) NaCl, (b) MgCl2, (c) CaCl2, and (d) $FeCl_3$.

Almost immediately after adding the salt, white precipitate was observed to form in all 4 solutions of HPAM. When HCl was added, none of the precipitates dissolved, indicating that the precipitate was polymeric. Furthermore, in beaker (d), white, sticky-looking globules of polymer was observed to have been formed. This can be better visualized in Figure 35 where the solution was emptied out to better show the precipitate formed.

Figure 35: Precipitated HPAM as a result of negative interactions with Fe^{3+} cation.

As can be observed from the HPAM precipitate formed, it is extremely sticky and viscous, which can result in plugged pore throats or the formation of filter cakes on the surface of the rock. This results in significant formation damage that can be difficult to resolve.

UV-VIS Spectrophotometry

Few papers have shown light scattering tests that show the effect of metal ions on FRs water. Metal ions force PAM-based FRs coil, so FRs will lose friction-reduction rate. The transmittance tests show how the pure HPAM FRs are affected by each salt solution. Fe^{3+}, Ca^{2+}, Mg^{2+} and Na^{+} are the representative metal ions that HPAM FRs can encounter during the whole procedure in a slickwater fracturing job. The transmittance of the sample can be calculated according to the following equation:

$$\%T = \frac{I}{I_0} * 100$$

Where I represents the intensity of light exiting the sample and I_0 represents the intensity of light striking the sample. In the experiment, wavelength used was 600nm. The HPAM concentration was 0.12 vol.% and the molecular weight of HPAM was around 12 million. Normalized transmittance data was used to eliminate the time effect of friction-solution change. The HPAM solution samples without salt were set to 100 and all the transmittance test results were normalized to these samples, allowing for a determination of which kind of salt affects the polymers more than others. Similarly, a less-damaging FR was compared under the same conditions as HPAM. The results for HPAM and the less-damaging FR are shown in Table 5 and Table 6 respectively.

Table 5: Transmittance results of HPAM FR solution with different salts

Salt	ppm	Concentration, w%	Molarity	Transmittance, %	Normalized Transmittance
$FeCl_3$	0	0	0.00	7	100.00
	10000	1	0.06	1	14.29
	42300	4.23	0.26	1.9	27.14
$CaCl_2$	0	0	0.00	5.2	100.00
	24200	2.42	0.22	6	115.38
	155900	15.59	1.40	11.3	217.31
$MgCl_2$	0	0	0.00	6.8	100.00
	51100	5.11	0.54	7.9	116.18
	209000	20.9	2.20	13.2	194.12
NaCl	0	0	0.00	7.3	100.00
	97100	9.71	1.66	11.3	154.79
	198800	19.88	3.40	17.3	236.99

Table 6: Transmittance results of the less-damaging FR solution with different salts

Salt	ppm	Concentration, w%	Molarity	Transmittance, %	Normalized Transmittance
$FeCl_3$	0	0	0.00	101	100.00
	6100	0.61	0.04	104	103.48
	29500	2.95	0.18	98	97.51
$CaCl_2$	0	0	0.00	101	100.00
	29800	2.98	0.27	98	97.51
	67600	6.76	0.61	93.6	93.13
$MgCl_2$	0	0	0.00	97.2	100.00
	35900	3.59	0.38	99.9	102.78
	57200	5.72	0.60	96.8	99.59
NaCl	0	0	0.00	99	100.00
	41100	4.11	0.70	100	101.01
	81500	8.15	1.39	99	100.00

The transmittance results indicate that with the same concentration, HPAM solutions have a lower transmittance value. Compared with water, the transmittance of HPAM solution with different salts is less than 20%, while the less-damaging FR solutions are almost the same, clear as Distilled (DI) water. Except for $FeCl_3$, the transmittance value becomes smaller as the metal ion concentration increases. Metal ions force polymers to bend or coil. Without salts, the HPAM polymers mostly relax in water.

Most light hits the polymers, and certain wavelength lights are absorbed, causing the transmittance to be low. As the HPAM polymers are forced to bend or coil as metal ion concentrations increase, more and more space becomes available for light to pass through. Therefore, the transmittance becomes smaller, and the solutions are clearer (Figure 36).

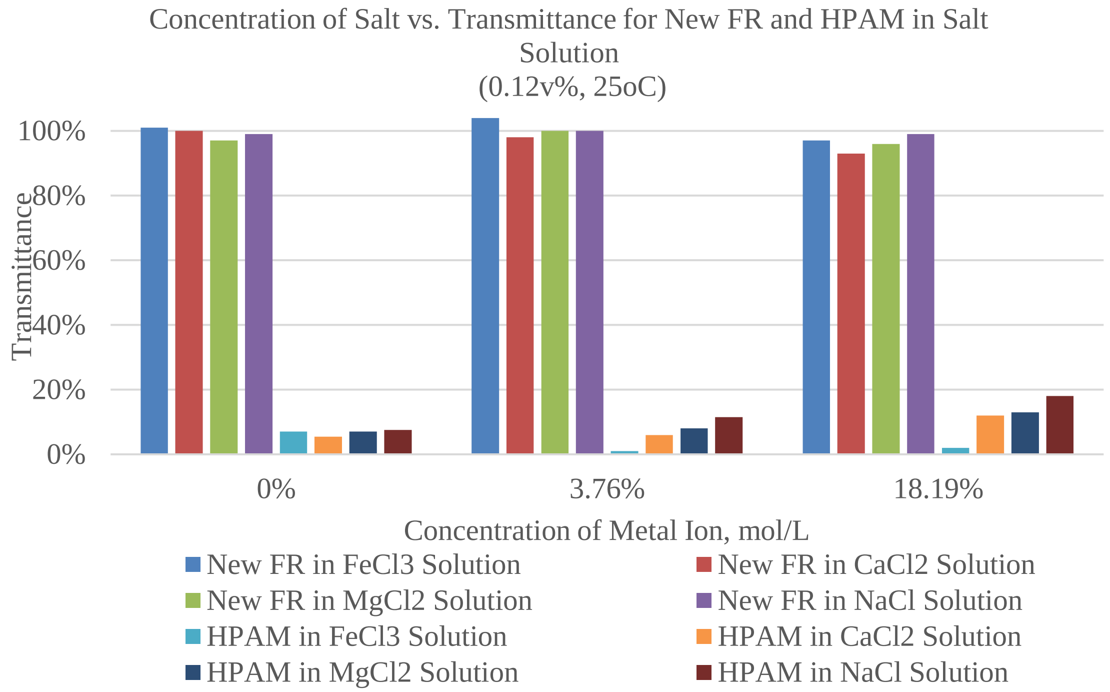

Figure 36: Transmittance results of the less-damaging FR vs. HPAM

Since the less-damaging FR solution does not have any large polymers, very few light beams can hit the polymers and be absorbed while penetrating the solutions. In ferric chloride solutions, HPAM reacted with ferric ions and flocculation formed, as shown in Figure 37. There is no flocculation for the less-damaging FR.

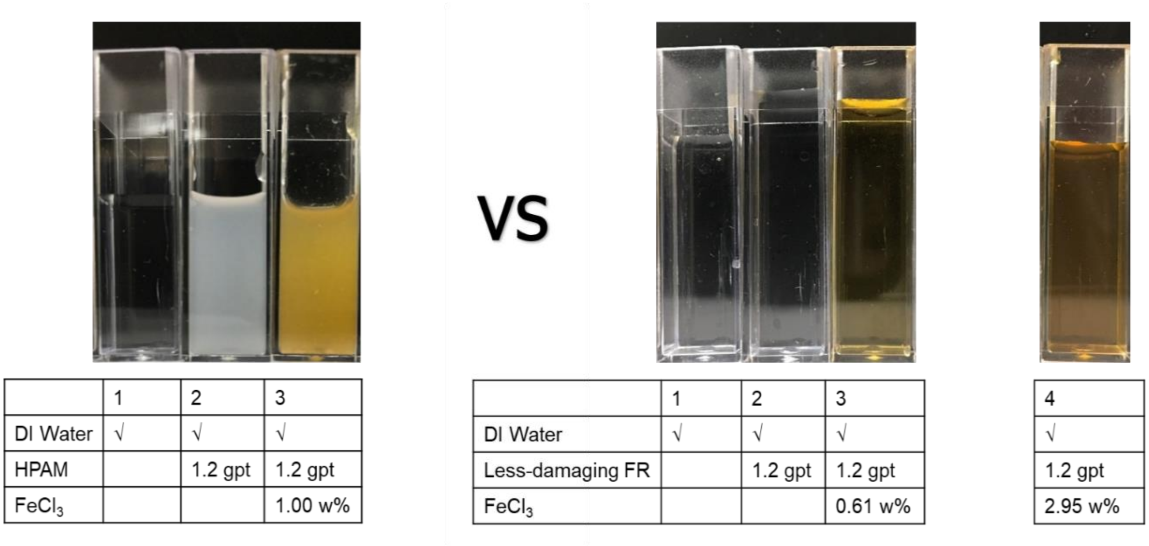

	1	2	3
DI Water	√	√	√
HPAM		1.2 gpt	1.2 gpt
$FeCl_3$			1.00 w%

	1	2	3
DI Water	√	√	√
Less-damaging FR		1.2 gpt	1.2 gpt
$FeCl_3$			0.61 w%

4
√
1.2 gpt
2.95 w%

Figure 37: HPAM vs. a less-damaging FR in $FeCl_3$ Solutions (HPAM: reacted with ferric ions and flocculated; Less-damaging FR: no flocculation)

In HPAM solutions with calcium chloride (Figure 38) and the ones with magnesium chloride (Figure 39), as the salt concentration increases, some little white dots can be observed. It could be the very early stage of flocculation.

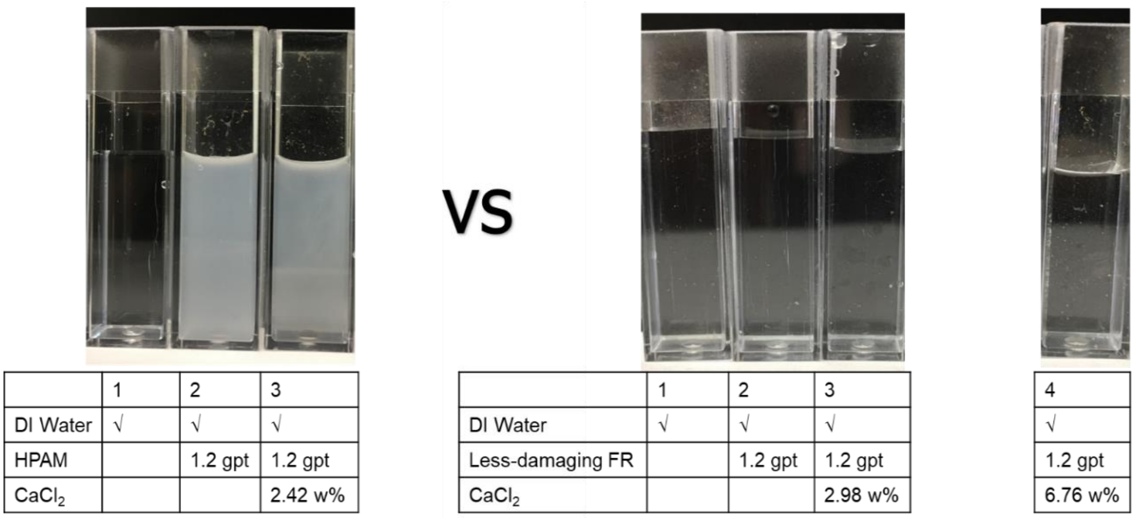

	1	2	3
DI Water	√	√	√
HPAM		1.2 gpt	1.2 gpt
$CaCl_2$			2.42 w%

	1	2	3
DI Water	√	√	√
Less-damaging FR		1.2 gpt	1.2 gpt
$CaCl_2$			2.98 w%

4
√
1.2 gpt
6.76 w%

Figure 38: HPAM vs. a less-damaging FR in CaCl2 solutions

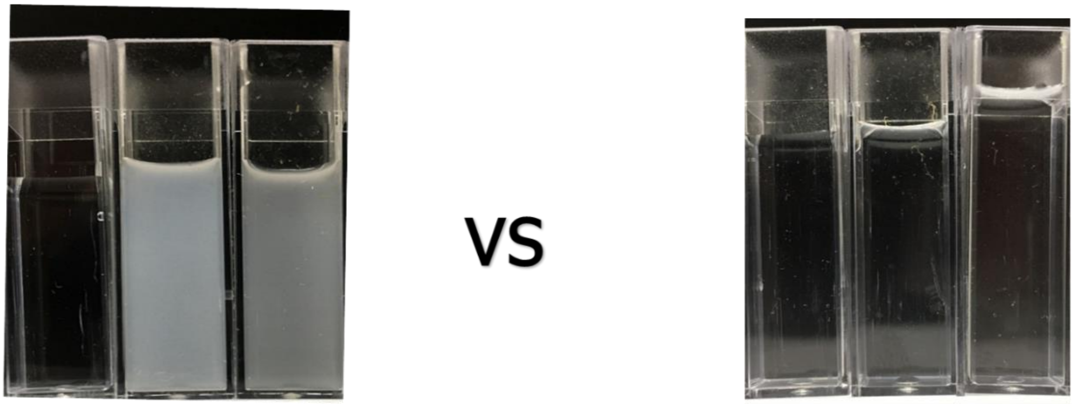

	1	2	3
DI Water	√	√	√
HPAM		1.2 gpt	1.2 gpt
$MgCl_2$			5.11 w%

	1	2	3
DI Water	√	√	√
Less-damaging FR		1.2 gpt	1.2 gpt
$MgCl_2$			5.72 w%

Figure 39: HPAM vs. a less-damaging FR in MgCl2 solutions

For all the salt solutions in tests, the less-damaging FR does not precipitate or flocculate. Excluding the $FeCl_3$ solution, the less-damaging FR's solutions remained clear, as shown in Figure 37 through Figure 40. Although, sodium chloride is one of the monovalent salts that affect polymers the least compared with divalent salts and trivalent salts. However, the colors of the solutions with different concentrations are different in Figure 37 through Figure 40. The background is black by design for better clarification of the flocculation process. The higher the concentration of NaCl is, the clearer the solution, i.e., the black background appears unobstructed. It means HPAM polymers stretch like barriers without NaCl, and the more Na^+, the more the polymers bend, so more space is available for light to pass through. The dark background (black) becomes more visible as sodium ion concentrations increase, as shown as Figure 40 (right), which indicates a clearer solution with fewer flocculates.

	1	2	3
DI Water	√	√	√
HPAM		1.2 gpt	1.2 gpt
NaCl			9.71 w%

	1	2	3
DI Water	√	√	√
Less-damaging FR		1.2 gpt	1.2 gpt
NaCl			8.15 w%

Figure 40: HPAM vs. a less-damaging FR in NaCl solutions

CHAPTER VII

VISCOSITY

For fracturing operations, proppant screenout in treatments is risky for wellbore integrity and equipment safe. Conventionally, viscosity is one of the most important variables for proppant suspension in fracturing fluid (Feng et al. 2017). Stokes' law was applied to designing most types of fracturing fluids, including guar-based fluids, cellulose-based fluids, and PAM-based fluids, in which the sedimentation velocity is inversely proportional to the medium viscosity. Later, the fluid elasticity was found to be another important variable that dominates proppant suspension (Harris and Harold 2000, Naval and Shah 2001; Hu 2015).

In slickwater fracturing in shale reservoirs, the mechanism of proppant transport is different. Since slickwater has only a small concentration of polymers (up to 2 gpt), it does not have high enough viscosity or elasticity required to keep the proppant in suspension. In this case, the proppant settles faster under static conditions, and proppant transport may be dominated by the movement of the proppant bank itself.

Three proppant transport mechanisms in slickwater have been proposed (Coker and Mack 2013; Sun 2015). At very low velocity, little or no proppant is moved. At higher velocity, proppant grains roll or slide along the surface of the settled proppant bank. At even higher velocity, proppant grains bounce off the surface back into the flow stream (saltation). Dufek and Bergantz (2007) demonstrated that saltation depends on the coefficient of restitution which is defined as the ratio of the velocity with which the object leaves after a collision to the velocity with which it enters the collision. Proppants with a higher coefficient of restitution and a lower friction coefficient than other proppants will be transported deeper into the fracture. Therefore, it is important to determine if the slickwater fracturing fluid has the necessary capabilities to suspend proppant despite the low concentration of polymer and friction reducer.

Viscosity Measurements

The viscosity of the HPAM and LDFR fluids were measured using two different machines. The first was a Grace M5600 viscometer that could operate at high pressure and high temperature conditions. 500 ml of 1.5 wt.% of each LDFR and HPAM was prepared and divided into 50 ml samples to be tested since this was the volume required by the viscometer for each test. Each friction reducer was tested by itself and in the presence of NaCl, $CaCl_2$, and $FeCl_3$. The shear rate was varied between 271 to 813 s^{-1}.

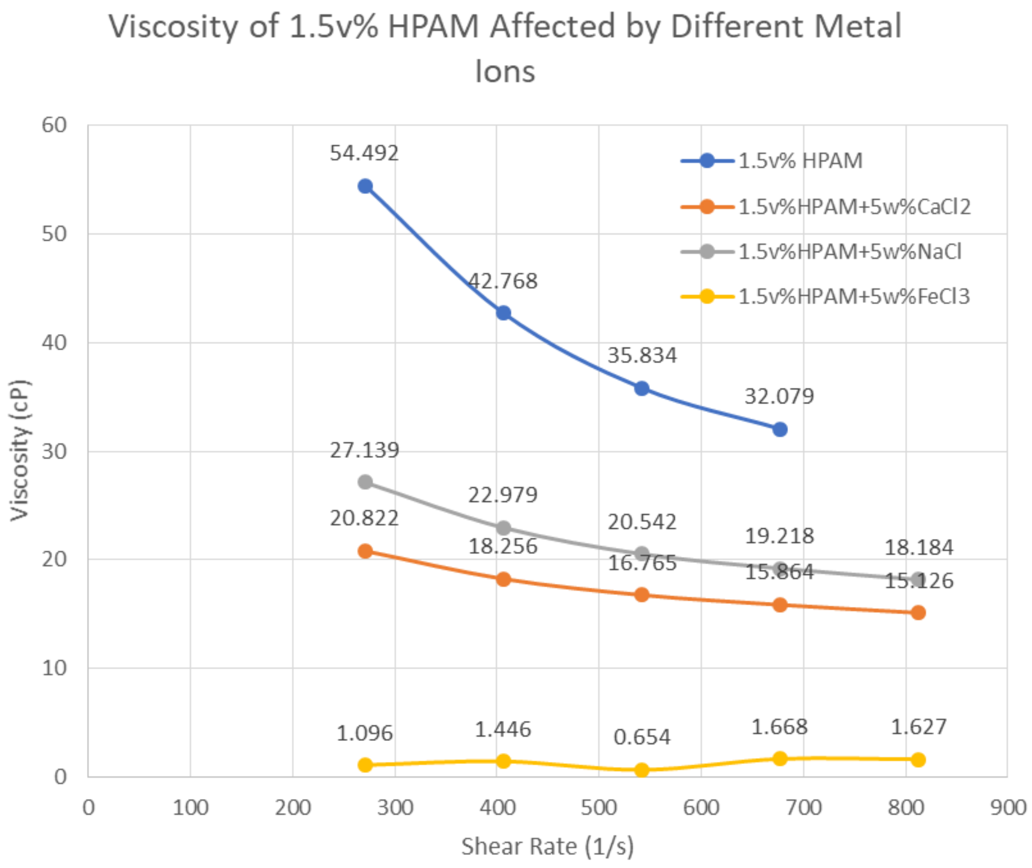

Figure 41: Viscosity vs shear rate for HPAM in the presence of different metal cations.

Figure 41 shows the effect of the different metal ions on the viscosity of HPAM. In the absence of any cations, the viscosity of HPAM alone is the highest, ranging from 32 to 54 cP depending on the shear rate. HPAM was also observed to be a shear thinning fluid, as the viscosity decreased as the shear rate increased. This property makes it ideal for pumping since slickwater fractures occur at high pump rates and the reduced HPAM viscosity at these rates would reduce pump and power requirements.

The addition of NaCl and $CaCl_2$ cation causes an approximately 50% decrease in the viscosity of the polymer solution while $FeCl_3$ causes the solution to lose all its viscosity. This is a result of coiling in the long chain HPAM polymer as the negatively charged sections of the polymer are attracted to the cations in solution. Viscosity of the solution is a result of the entanglement of long chain polymers. Since HPAM is coiled in the presence of cations, it is no longer able to entangle with other HPAM chains, causing the solution's viscosity to decrease. Furthermore, since straightened polymers are required in order to reduce the movement of turbulence from the wall, coiled HPAM will be unable to provide significant friction reducing properties.

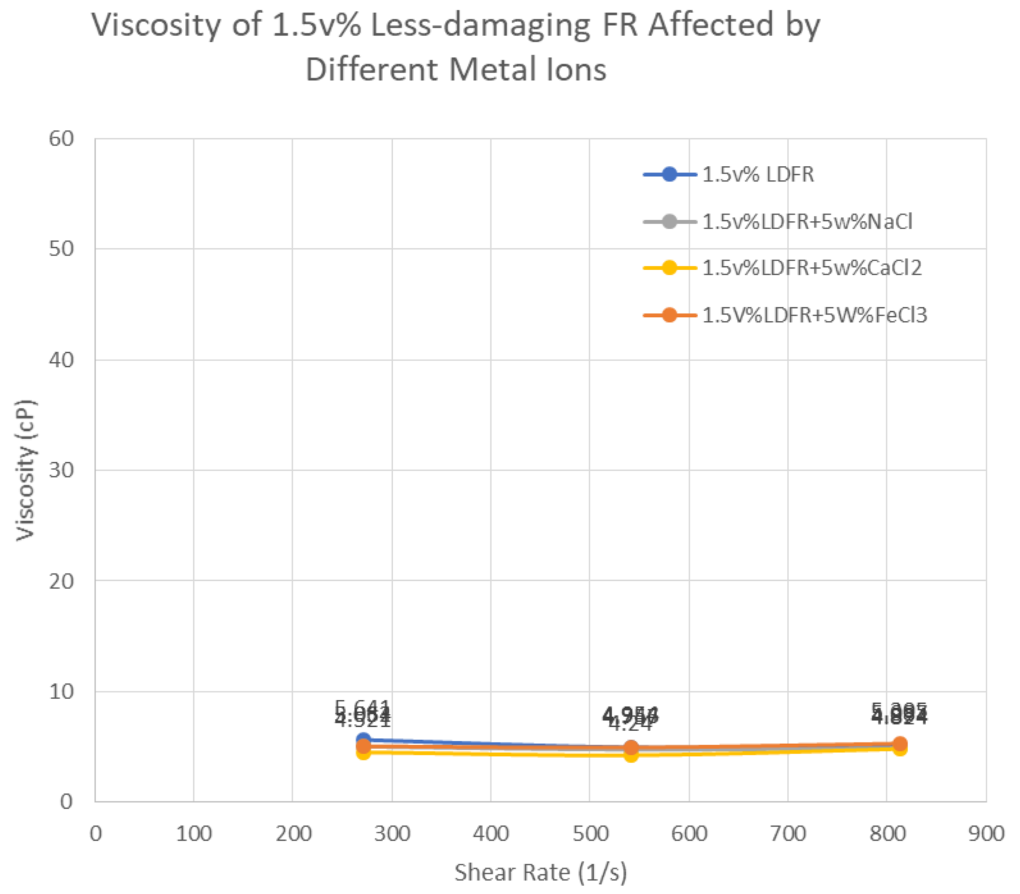

Figure 42: Viscosity vs shear rate for LDFR in the presence of different metal cations.

The results of the viscosity tests of LDFR are shown in Figure 42 above. Despite the addition of salts to the LDFR, its viscosity was not affected as it remained relatively similar between the tests. This meant that the LDFR did not undergo any coiling or have any negative interaction with the salts added. This would allow the LDFR to continue performing well despite the presence of salts. Furthermore, increasing the shear rate appeared to have no effect on the viscosity of the LDFR with its viscosity values holding constant in the presence of ions.

The viscosity tests were then repeated on a RheoSense m-VROC micro viscometer. Due to the method of measurement, this viscometer was able to generate much higher shear rates and required a significantly lower volume of test solution (50 µl) as compared to the Grace M5600 viscometer (50 ml). The same solution of HPAM that was used for the earlier viscosity test was used for this set of tests. Similarly, the concentrations of NaCl, $CaCl_2$, and $FeCl_3$ were kept the same as before.

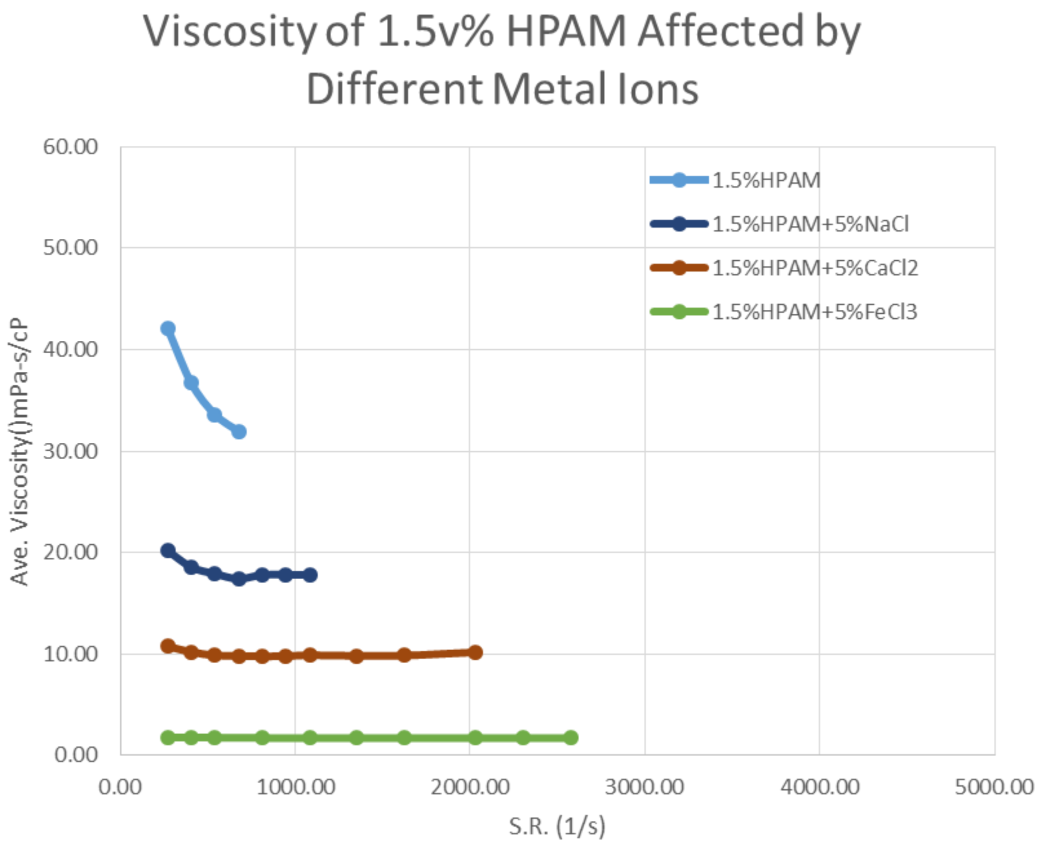

Figure 43: Viscosity vs shear rate for HPAM in the presence of different metal cations measured by micro viscometer.

The results for HPAM from the micro viscometer are shown in Figure 43. Just like in the previous viscometer test, it can be seen that the addition of salt to the HPAM solution significantly reduces the viscosity. This confirms the negative influence of salt on the viscosity of HPAM, which indicates a similar negative effect on the friction reducing properties of the polymer.

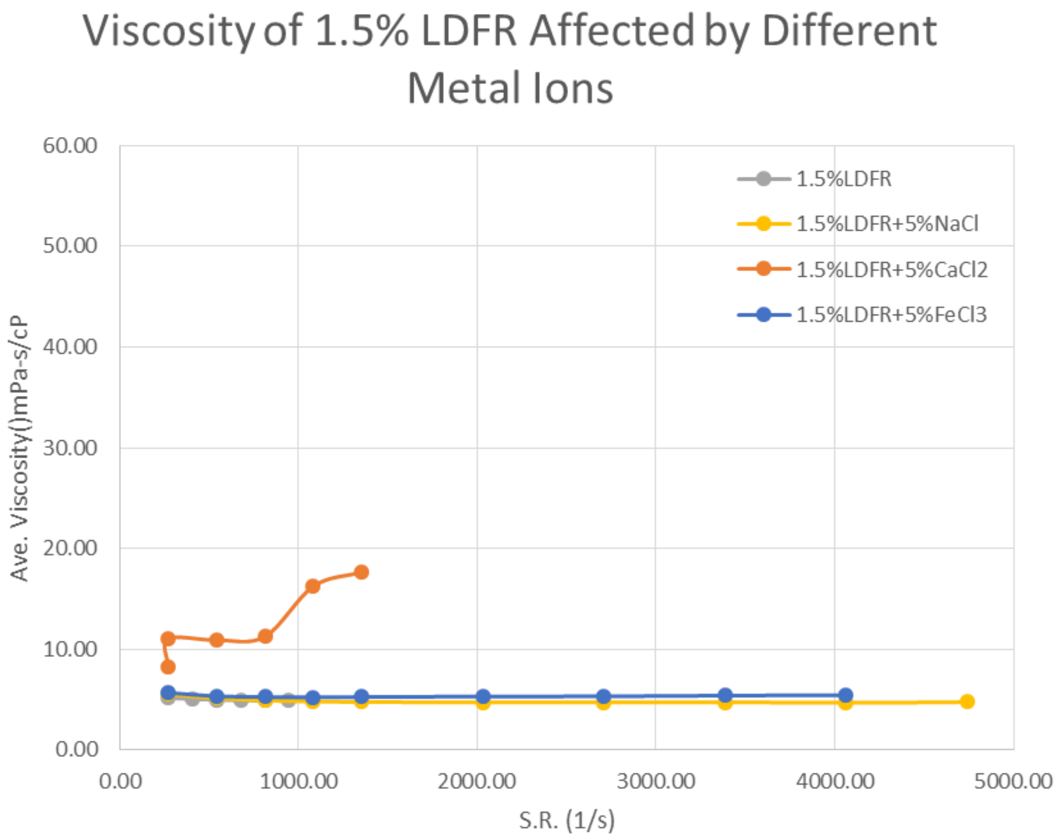

Figure 44: Viscosity vs shear rate for LDFR in the presence of different metal cations measured by micro viscometer.

The results for the LDFR are shown in Figure 44. As before, the LDFR was shown to be generally unaffected by the metal cations added. The viscosities did not change with shear rate or the type of metal ion added, unlike that of HPAM. However, an anomaly was observed for the solution containing $CaCl_2$ where the viscosity of the solution was observed to increase. Further examination of the equipment revealed that the cause of this anomalous reading was a white precipitate that was present in the syringe of the micro viscometer as shown in Figure 45.

Figure 45: Precipitation in the micro viscometer from LDFR solution with $CaCl_2$.

The white precipitate was removed from the syringe and placed in a beaker to which HCl was added. The precipitate was observed to dissolve completely with the addition of HCl and was concluded to be $Ca(OH)_2$. This observation was similar to that made earlier during precipitation tests when $CaCl_2$ was added to LDFR, indicating that care must be taken to adjust the pH of the LDFR solution in order to prevent precipitation of any basic Ca^{2+} salts in the formation during the treatment.

CHAPTER VIII

COREFLOOD EXPERIMENTS

Formation Damage

The goal of hydraulic fracturing is to maximize production, the extent of which is directly linked to how much the formation is damaged after fracking. Therefore, it is important to determine the extent of formation damage caused by the friction reducers after they are pumped. A highly damaged formation will result in reduced production despite the fracturing treatment. Therefore, core flood tests were carried out using Carbon Tan sandstone cores as they represent a variety of formations and are extremely commonly used.

A pressure transducer connected to the inlet and outlet of the core holder measures the pressure drop across the core. This indicates the extent of formation damage caused by the polymer since a high pressure drop indicates blocked pore spaces and the inability of the fluid to pass through the core. HPAM and the less-damaging friction reducer (LDFR) were compared with and without $FeCl_3$. Each core was first flooded with 8 wt.% KCl in order to establish a baseline before 1.5 wt.% of each FR solution was pumped.

First, HPAM was compared to LDFR as shown in Figure 46 in the absence of $FeCl_3$. From the figure, it can be seen that both FR solutions have the same initial pressure drop as 8 wt.% KCl solution. As the injection continues, a spike in the pressure drop across the core was observed. This was expected since HPAM is a long chain polymer while the LDFR is composed of smaller, shorter chain surfactants.

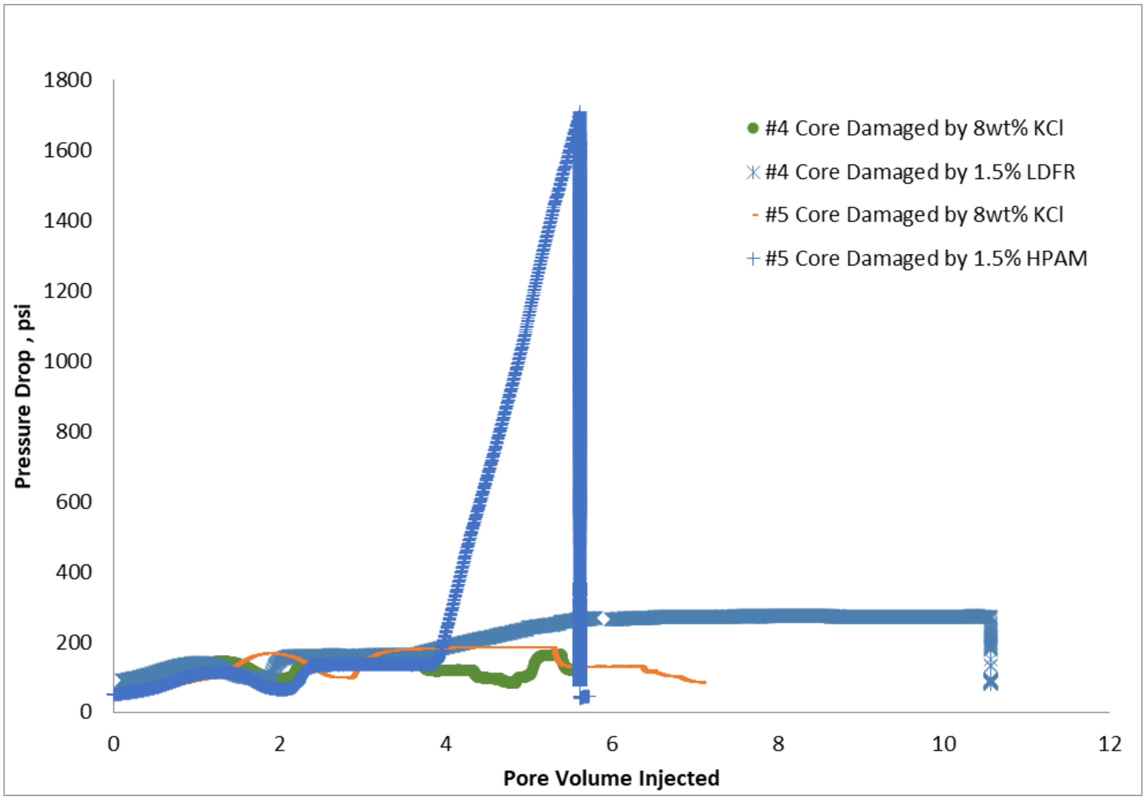

Figure 46: Core flood tests with HPAM and LDFR.

The sharp decrease in the pressure drop observed after almost 6 PVs of HPAM was injected is likely due to the core fracturing as a result of the high pressure drop. On the other hand, the core flooded with LDFR showed only a slight increase in pressure drop. This indicates that the LDFR is less damaging than HPAM.

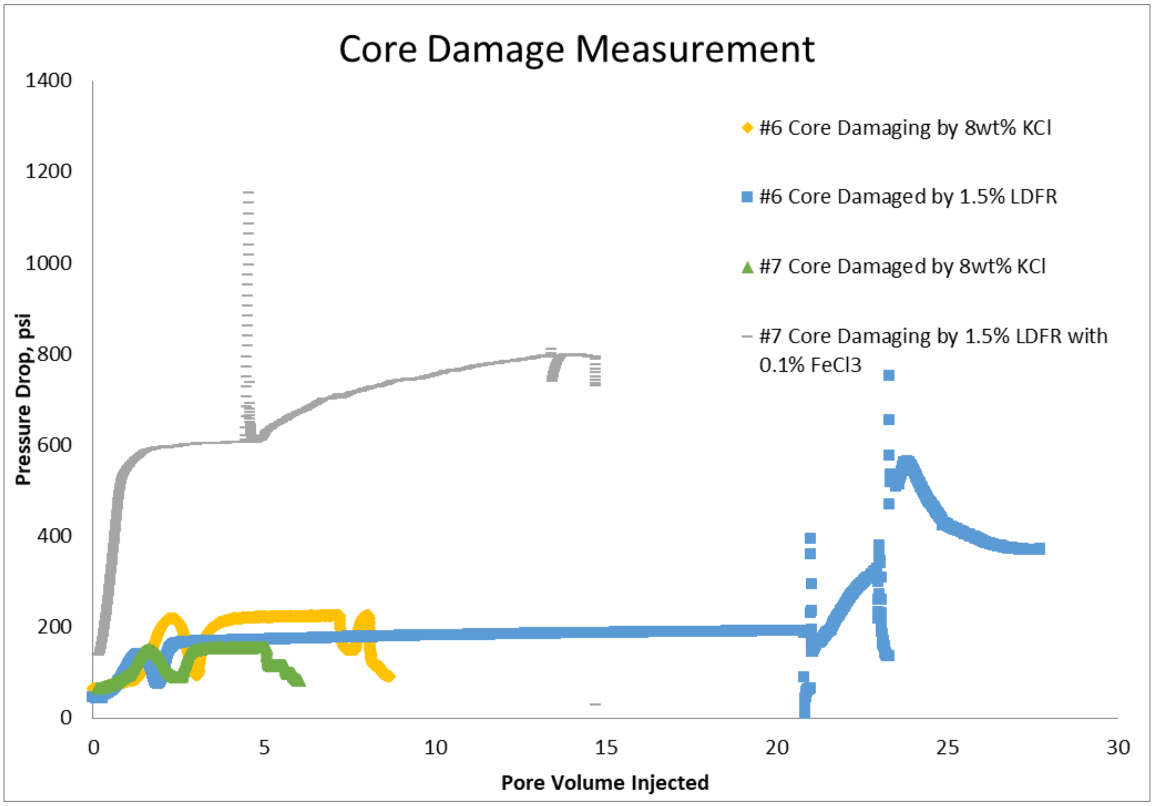

Figure 47: Core flood tests with LDFR in the presence of $FeCl_3$.

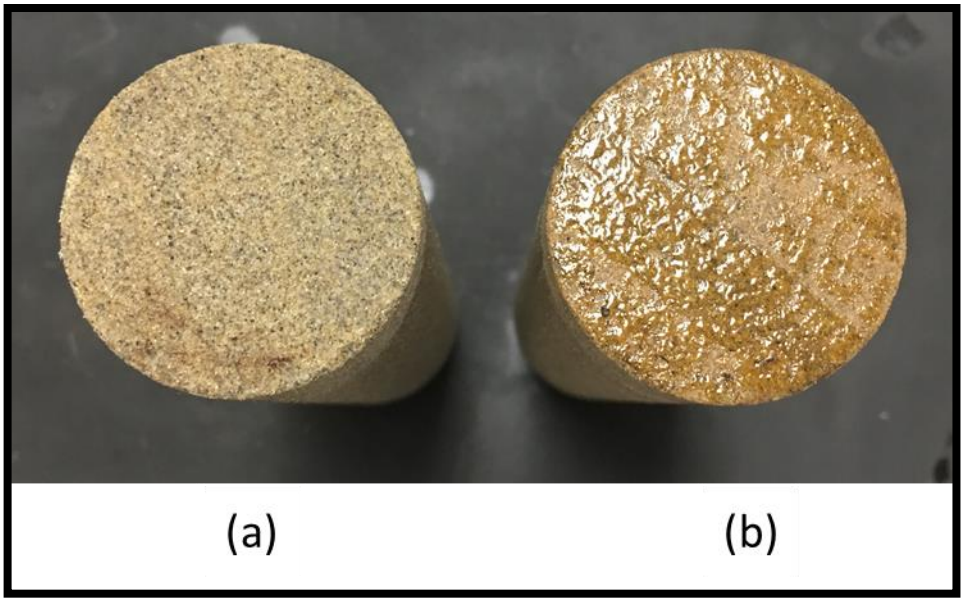

Figure 48: Core faces after LDFR core flood tests. (a) Did not have $FeCl_3$ while (b) contained 0.1 wt.% $FeCl_3$.

Next, core flood tests were carried out with the same polymers and $FeCl_3$. This salt was chosen as Fe^{3+} is known to have strong interactions with polymers and surfactants, often causing flocculation and forming precipitates with these molecules that result in significant formation damage. Figure 47 shows the performance of the LDFR test in the presence and absence of $FeCl_3$. As expected, the presence of $FeCl_3$ significantly increases the pressure drop across the core as the LDFR interacts negatively with the Fe^{3+} ions present. Figure 48 shows the core faces after the core flood test. As can be observed in the test with $FeCl_3$, some residue remains on the surface of the core.

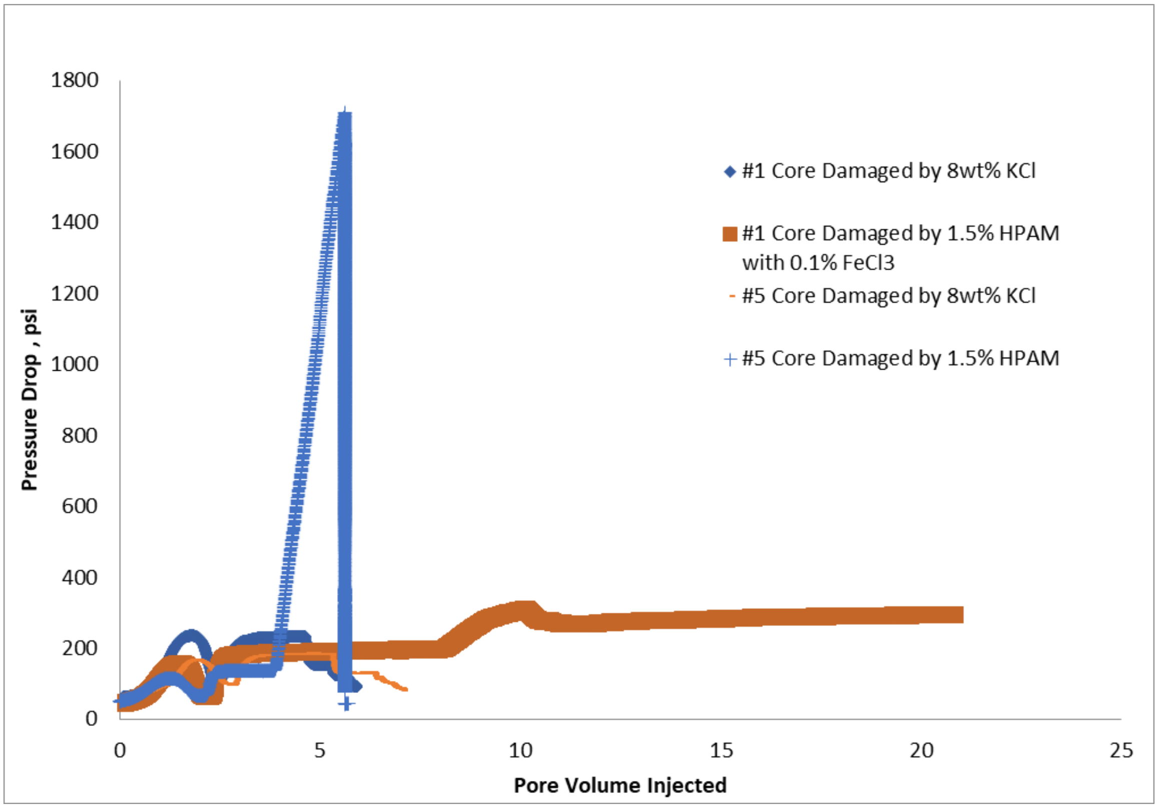

Figure 49: Core flood tests with HPAM in the presence of $FeCl_3$.

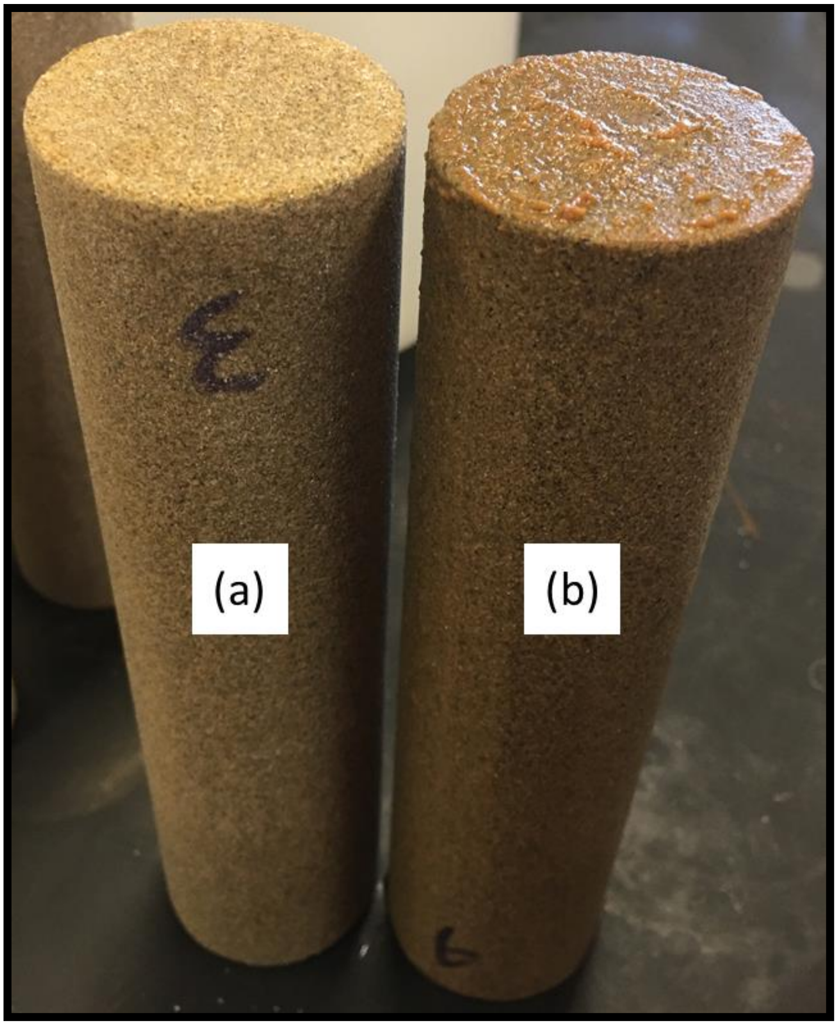

Figure 50: Core faces after HPAM core flood tests. (a) Did not have $FeCl_3$ while (b) contained 0.1 wt.% $FeCl_3$.

The same set of tests were then carried out with HPAM and shown in Figure 49. However, unlike the core flood tests with LDFR, HPAM with $FeCl_3$ showed better performance than in the absence of Fe^{3+} ions. This is likely due to the precipitation of the polymer in the accumulator. As a result, the fluid that was pumped through the core did not contain any polymer as the precipitated polymer would have been unable to pass through the lines of the core flood setup. The damage from the interaction between

HPAM and $FeCl_3$ can be seen in Figure 50. By examining the face of the core in Figure 50b, shreds of polymer can be seen on the surface of the core.

Effect on Proppant

Placing proppant is part of a slickwater fracturing treatment to prevent the mouth of the fracture from closing after the treatment. The spaces between the proppant allow for the flow of hydrocarbons from the formation to the wellbore, thereby facilitating their production. As a result, it is important to examine if the slickwater fracturing fluid will leave any residue or cause plug the propped-up fracture after the treatment is complete. To achieve this, hollow stainless-steel cores were packed with different sizes of synthetic quartz proppant and the slickwater fluid was passed through them.

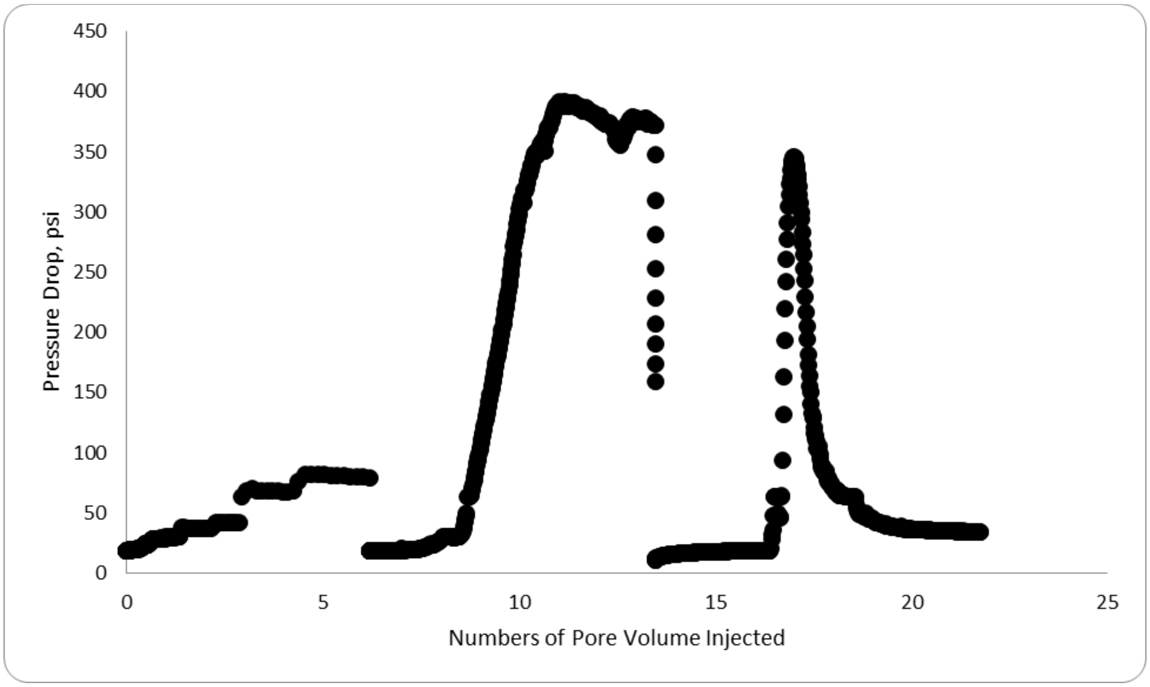

Figure 51: 20-40 mesh synthetic quartz proppant after core flood with 1.5 wt.% HPAM.

Figure 51 shows the pressure drop in the core after 1.5 wt.% of HPAM solution was passed through it. As can be seen, significant pressure drops were observed when approximately 10 and 17 pore volumes of HPAM solution were injected. This is likely due to some formation damage as the HPAM is passing through the proppant with the sharp decrease in pressure drops indicating that the damage was relieved or that new paths were found through the proppant.

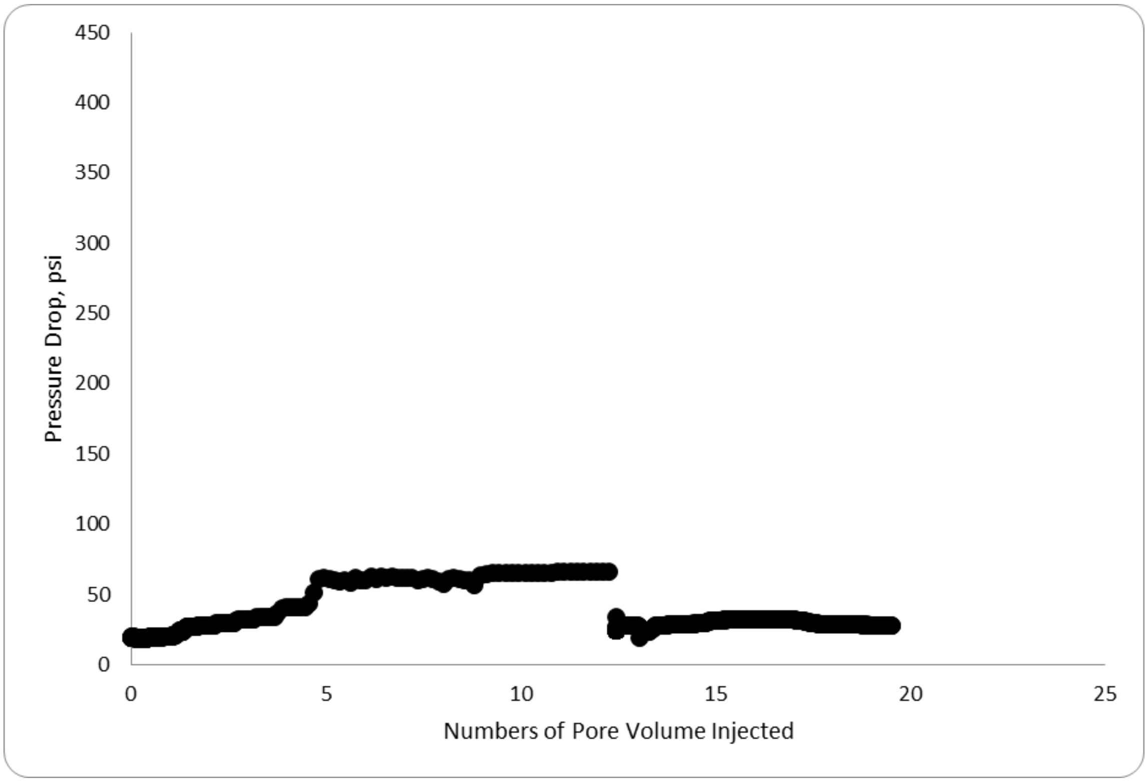

Figure 52: 20-40 mesh synthetic quartz proppant after core flood with 1.5 wt.% LDFR.

When the LDFR was tested however, the significant pressure drops observed with HPAM were not seen as shown in Figure 52. The core flood test with LDFR showed little to no pressure drop as the fluid passed through the core. This is likely due to the small molecular size of the LDFR components compared to the large, long chain polymer that is HPAM.

Next, cores containing 40-70 mesh proppant was used. These proppants are smaller in size compared to the previous 20-40 mesh proppant with a particle size range between 212 and 420 µm.

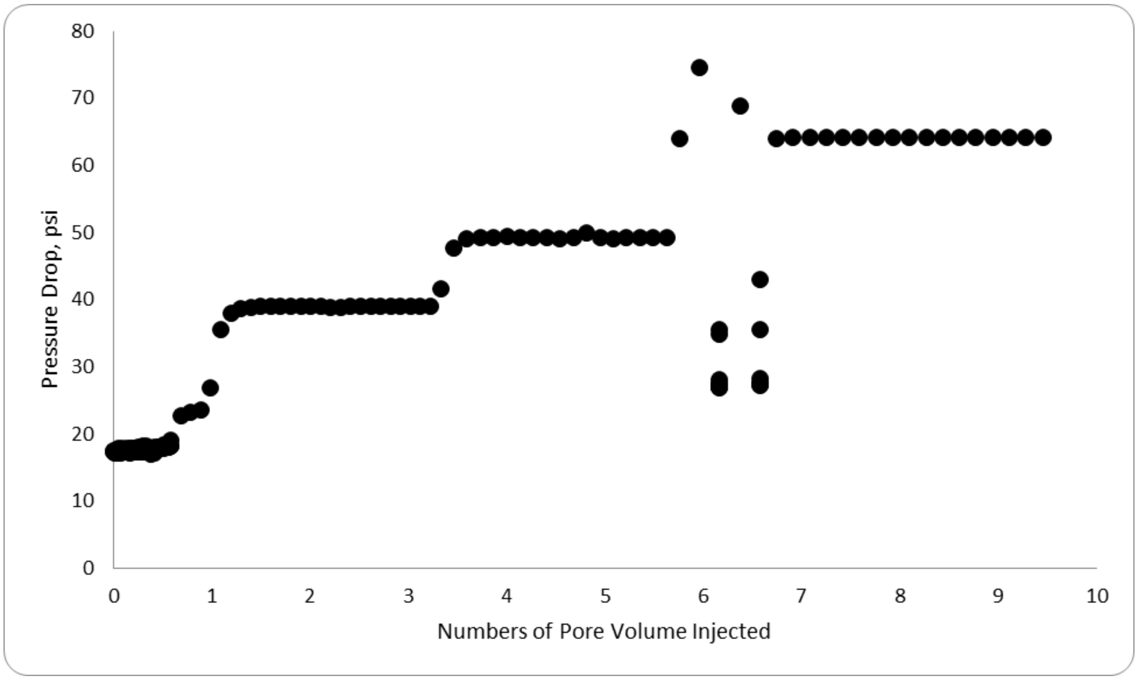

Figure 53: 40-70 mesh synthetic quartz proppant after core flood with 1.5 wt.% HPAM.

Figure 53 shows the core flood test results of pumping 1.5 wt.% HPAM solution through 40-70 mesh proppant. For these higher mesh size proppant packs, the flow rate was increased stepwise in order to check for abrupt spikes in pressure drop readings which would indicate some blockage. This was observed when HPAM was passed through the 40-70 mesh core as shown in Figure 53.

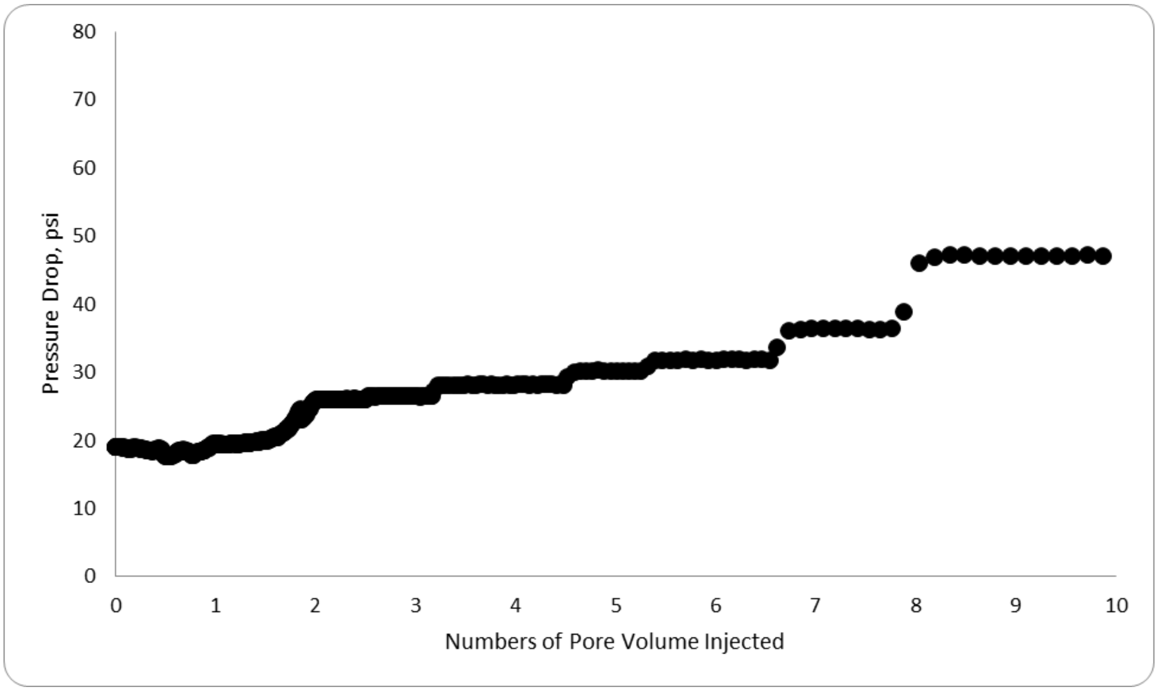

Figure 54: 40-70 mesh synthetic quartz proppant after core flood with 1.5 wt.% LDFR.

The 1.5 wt.% LDFR solution was then pumped through the 40-70 mesh proppant core. As can be observed in Figure 54, each time the flow rate of LDFR is increased, the pressure drop increases and is maintained with no interruptions. This shows that the LDFR will not create any blockage during flowback after the fracture treatment is completed.

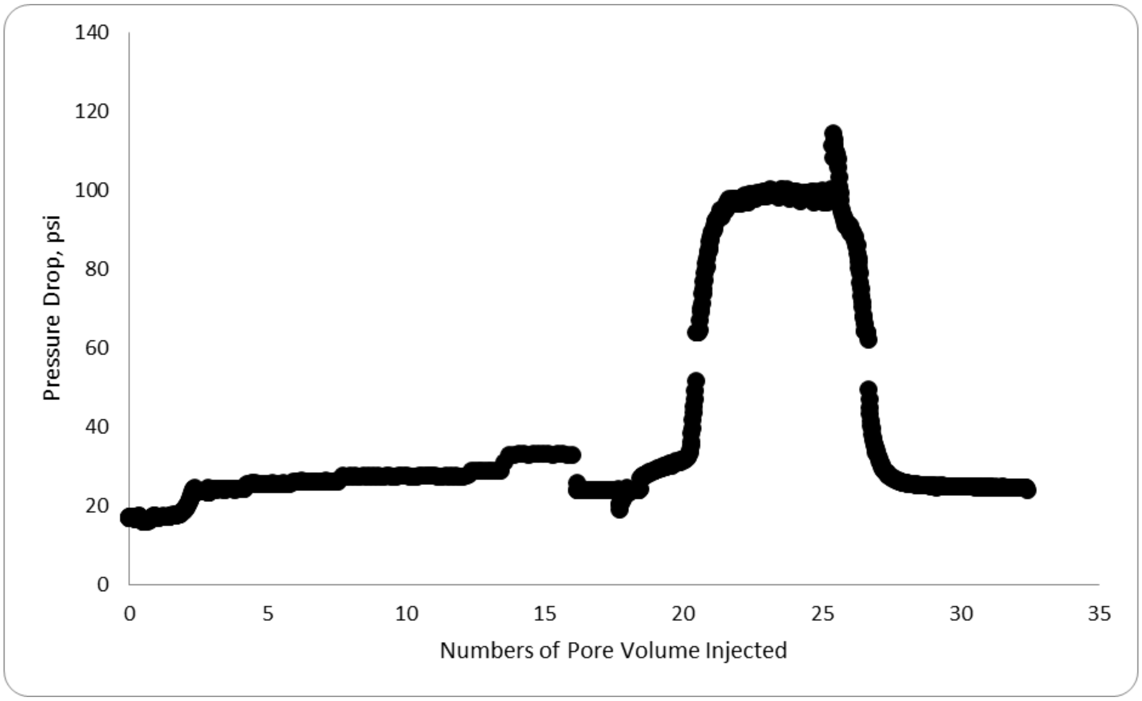

Figure 55: 100 mesh synthetic quartz proppant after core flood with 1.5 wt.% HPAM.

The final set of core flood tests were carried out using 100 mesh synthetic quartz proppant. This proppant is the smallest of the more commonly used sizes of proppant. When the HPAM solution was injected as shown in Figure 55, it can be seen that at approximately 20 pore volumes, a spike in the pressure drop was observed. As seen in the previous core flood experiments using HPAM, this observation is likely due to a blockage formed due to the HPAM polymer, thereby causing a spike in the pressure drop.

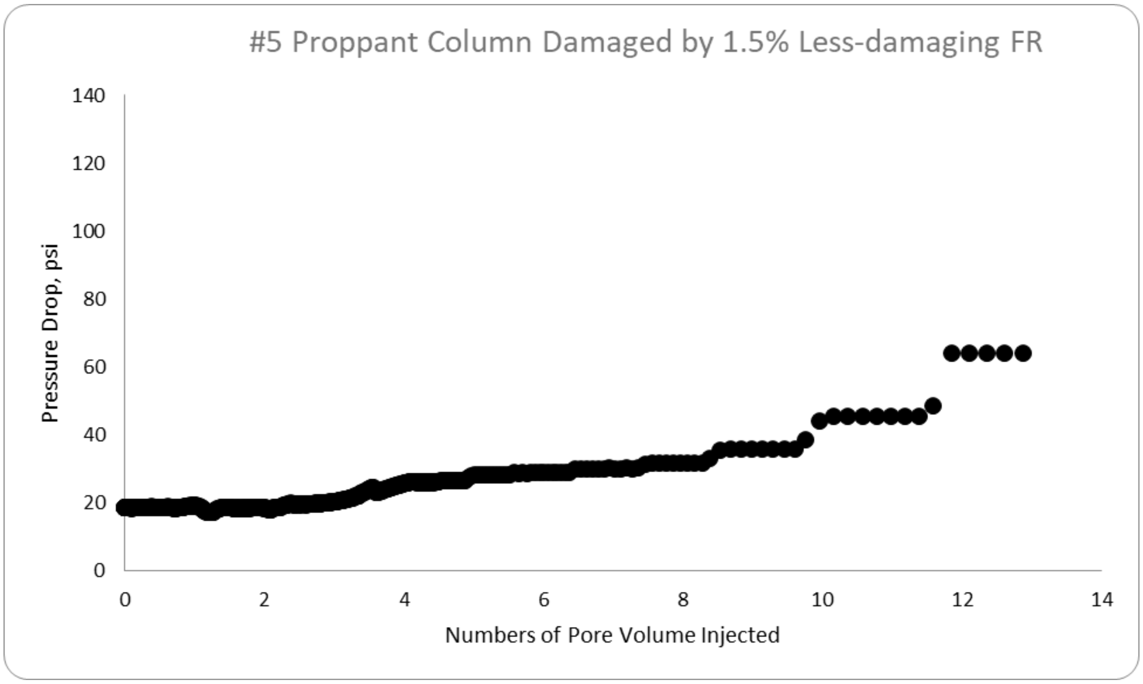

Figure 56: 100 mesh synthetic quartz proppant after core flood with 1.5 wt.% LDFR.

Figure 56 shows the pressure drop measured when 1.5 wt.% LDFR solution was injected into a 100-mesh synthetic quartz core. As can be observed, there were no spikes in the pressure drop as the flow rate was increased with the changes being stepwise and the pressure drops remaining constant at each step. This indicates that the LDFR, as shown in previous core flood tests, does not cause significant formation damage to the fracture after the treatment is complete.

Regained Permeability

Furthermore, it is necessary to carry out core flood experiments prior to fracturing treatment in order to determine the regained permeability of the core.

The LDFR was compared to commercial HPAM FRs to determine the extent of formation damage. 2 solutions of HPAM were prepared for this experiment at a concentration of 1.5 wt.% each. FR-A is a commercial dry powder FR, and FR-B is a regular emulsion FR. When tested, these solutions lead to less than 10% regained permeability while the less-damaging FR saw 99.2% regained permeability after the core flood as shown in Table 7. In the table, K_1 (md) refers to the initial permeability, while K_2 is the regained permeability. From this test, it can be seen that the LDFR has a smaller effect on the permeability of the core after the treatment, indicating lower formation damage and, as a result, high productivity.

Table 7: Core flood results comparison between less-damaging FR to common commercial FRs without breakers

FRs	K_1 (md)	K_2 (md)	Regained Permeability
FR-A	172.7	12.76	7.4%
FR-B	166.3	0.5	0.3%
LDFR	147.7	146.5	99.2%

CHAPTER IX

FIELD TESTS

In order to validate the applicability of the LDFR, it was necessary to carry out field tests with it. From the laboratory tests shown earlier, it can be observed that the LDFR performs well under artificial conditions. The field tests would therefore allow for proper evaluation of the LDFR.

Comparative daily gas production through two wells on the same platform: one well was fractured using a slickwater with less-damaging FR (Gas Well #1) and the other by a conventional inverse emulsion FR (Gas Well #2)) (Figure 57).

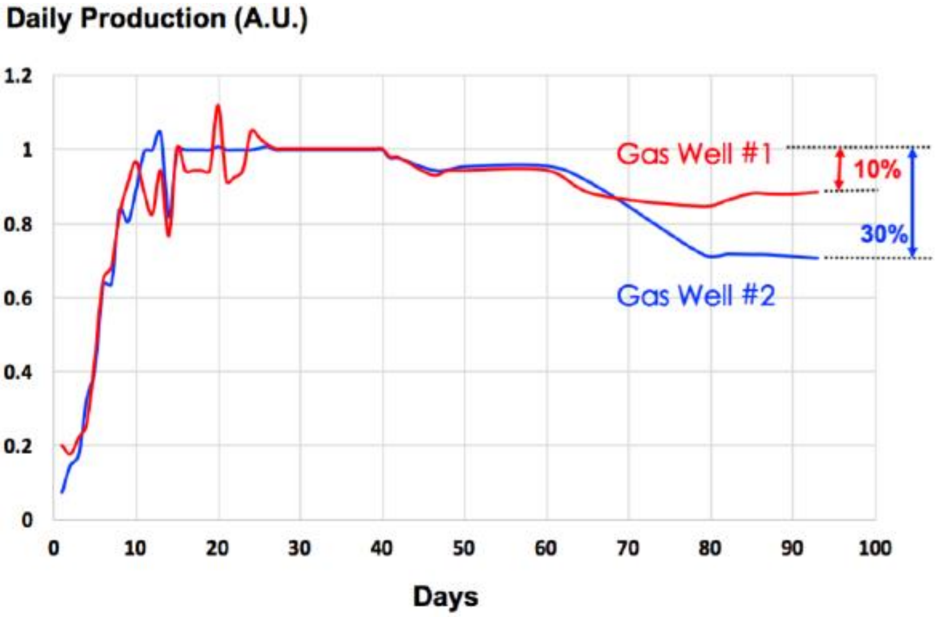

Figure 57: Gas production rate: Less-damaging FR (red) vs. conventional FR (blue)

Results show that the less-damaging FR is three times more effective at increasing daily gas production than conventional inverse emulsion FR. For gas well #1, the decline rate was 10% after three months of production. On the other hand, gas well #2 had a decline rate of 30% after three months of production.

When comparing the production regime of gas well #2 production to statistical data, large similarities can be observed. The literature reports an average of 30% decline after three months of gas production on 838 wells (Figure 58). This matches the decline in production rate observed in gas well #2. This is much higher than the well fractured by slickwater with the LDFR which only had a decline of 10% of gas production, likely as a result of lower formation damage of the LDFR.

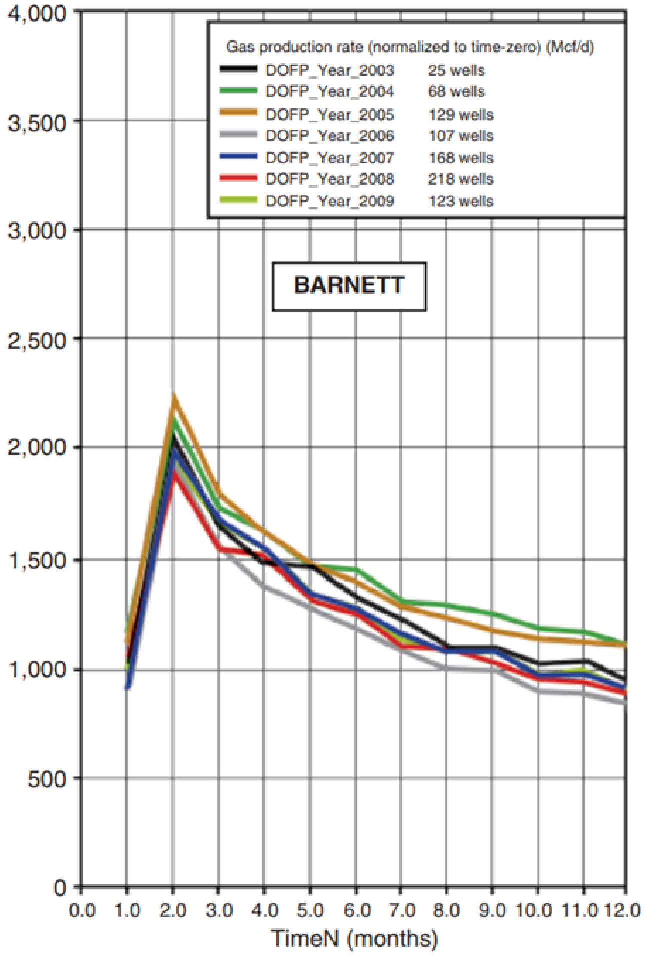

Figure 58: Barnett shale first-year production rates

CHAPTER X

CONCLUSIONS

In conclusion, the commercial, polymer-based friction reducers such as polyacrylamide can cause significant formation damage due to its large molecular size, as well as its severely negative interactions with metal cations present in the formation. As such, a new less-damaging friction reducer formula was designed from short chain polymers and surfactants as a replacement. It can therefore be concluded that:

1. MD simulations were able to explain how the commonly used FRs interact with different metal ions in water.
2. Both MD simulations and precipitation tests show that HPAM is most sensitive to Fe^{3+}, then Ca^{2+}/Mg^{2+}, then Na^{+}/K^{+}. This is consistent with the typical FR performance.
3. Reducing ferric (by reducing agents) to ferrous minimizes the negative influence of iron cations, which is also consistent with our MD simulations.
4. Potential formation damage caused by FRs in slickwater is confirmed by both MD simulations and lab tests (UV-vis tests and core flood tests).
5. The core flood and field results show that the LDFR is has better performance than commercial FRs.
6. By combining molecular dynamics simulation, lab tests, and field tests, a more effective FR is found for slickwater with high salt-tolerant, almost non-damage to formations and more gas production.

REFERENCES

Alkouh, Ahmad Bader, Mcketta, Steven F, and Wattenbarger, Robert A. 2013. Estimation of fracture volume using water flowback and production data for shale gas wells. *Proc.*, SPE Annual Technical Conference and Exhibition.

Banerjee, S., Abdulsattar, Z., Agim, K. et al. 2017. Mechanism of polymer adsorption on shale surfaces: Effect of polymer type and presence of monovalent and divalent salts. *Petroleum* **3** (3): 384-390. http://dx.doi.org/10.1016/j.petlm.2017.04.002.

Barati, R. and Liang, J. 2014. A Review of Fracturing Fluid Systems Used for Hydraulic Fracturing of Oil and Gas Wells. *Journal of Applied Polymer Science* **131**(16):1-9. http://doi.org/10.1002/app.40735.

Barati, R., Johnson, S., McCool, S. et al. 2011. Fracturing fluid cleanup by controlled release of enzymes from polyelectrolyte complex nanoparticles. *Journal of Applied Polymer Science* **121** (3): 1292-1298. http://dx.doi.org/10.1002/app.33343.

Barati, Reza, Johnson, Stephen J, McCool, Stan et al. 2011. Fracturing fluid cleanup by controlled release of enzymes from polyelectrolyte complex nanoparticles. *Journal of Applied Polymer Science* **121** (3): 1292-1298.

Carman, P.S. and Cawiezel, K.E. 2007. Successful Breaker Optimization for Polyacrylamide Friction Reducers Used in Slickwater Fracturing. Presented at the SPE Hydraulic Fracturing Technology Conference, College Station, Texas, USA, 29-31 January. SPE-106162-MS. http://doi.org/10.2118/106162-MS.

Cipolla, C. and Wallace, J. 2014. Stimulated Reservoir Volume: A Misapplied Concept?. Presented at the SPE Hydraulic Fracturing Technology Conference, The Woodlands, Texas, USA, February 4–6. https://doi.org/10.2118/168596-MS.

Dill, W. and Smolarchuk, P. 1988. Iron Control in Fracturing and Acidizing Operations. *J Can Pet Technol* **27**(03). PETSOC-88-03-08. https://doi.org/10.2118/88-03-08.

Dusseault, Maurice and McLennan, John. 2011. Massive multistage hydraulic fracturing: Where are we. *Proc.,* 45th US Rock Mechanics/Geomechanics Symposium.

EIA. 2019. Annual Energy Outlook 2019 with projections to 2050, U.S. Department of Energy, https://www.eia.gov/outlooks/aeo (January, 2019).

Essington, M. E. 2005. Soil and Water Chemistry: An Integrative Approach.: CRC Press.

Goswick, R. A. and LaRue, J. L. 2014. Utilizing Oil Soluble Tracers to Understand Stimulation Efficiency Along the Lateral. Presented at the SPE Annual Technical Conference and Exhibition, Amsterdam, The Netherlands, October 27–29. https://doi.org/10.2118/170929-MS.

Gubian, Emilie. Changes in shale well design: Reaching the limits? *IHS Markit*, https://ihsmarkit.com/research-analysis/changes-in-shale-well-design-reaching-the-limits.html.

Guo, J., Li, Y., and Wang, S. 2018. Adsorption damage and control measures of slick-water fracturing fluid in shale reservoirs. *Petroleum Exploration and Development* **45** (2): 336-342. http://dx.doi.org/10.1016/s1876-3804(18)30037-5.

Hofmann, H., Babadagli, T., and Zimmermann, G. 2014. Numerical Simulation of Complex Fracture Network Development by Hydraulic Fracturing in Naturally Fractured Ultratight Formations. *Journal of Energy Resources Technology* **136** (4): http://dx.doi.org/10.1115/1.4028690.

Holloway, M. D. and Rudd, O. 2013. Production Development. Fracking: The Operations and Environmental Consequences of Hydraulic Fracturing., Scribner.

Ibrahim, A. F., Nasr-El-Din, H. A., Rabie, A., et al. 2018. A New Friction-Reducing Agent for Slickwater-Fracturing Treatments. *SPE Prod & Oper* **33**(03): 583 - 595. SPE-180245-PA. https://doi.org/10.2118/180245-PA.

Jackson, R. B., Osborn, S., Vengosh, A. et al. 2011. Reply to Davies: Hydraulic Fracturing Remains a Possible Mechanism for Observed Methane Contamination of Drinking Water. Presented at the Proceedings of the National Academy of Sciences, October 25, 2011. https://doi.org/10.1073/pnas.1113768108.

Jin, X., Shah, S. N., Roegiers, J. et al. 2015. An Integrated Petrophysics and Geomechanics Approach for Fracability Evaluation in Shale Reservoirs. *SPE J.* **20** (03): 518-526. https://doi.org/10.2118/168589-PA.

Joshi, Sada D. 1991. *Horizontal well technology*: PennWell Books.

Kaşgöz, H., Özgümüš, S., and Orbay, M. 2003. Modified Polyacrylamide Hydrogels and Their Application in Removal of Heavy Metal Ions. *Polymer* **44**(6): 1785–1793. https://doi.org/10.1016/S0032-3861(03)00033-8.

King, G. E. 2010. Thirty Years of Gas Shale Fracturing: What Have We Learned?. Presented at the SPE Annual Technical Conference and Exhibition, Florence, Italy, September 19–22. https://doi.org/10.2118/133456-MS.

King, G. E. 2012. Hydraulic Fracturing 101: What Every Representative, Environmentalist, Regulator, Reporter, Investor, University Researcher, Neighbor and Engineer Should Know About Estimating Frac Risk and Improving Frac Performance in Unconventional Gas and Oil Wells. Presented at the SPE Hydraulic Fracturing Technology Conference, The Woodlands, Texas, USA, February 6–8. https://doi.org/10.2118/152596-MS.

Kuila, U. and Prasad, M. 2011. Understanding Pore-Structure and Permeability in Shales. Presented at the SPE Annual Technical Conference and Exhibition, Denver, Colorado, USA, 30 October-2 November. SPE-146869-MS. https://doi.org/10.2118/146869-MS.

Lindsay, G. J., White, D. J., Miller, G. A. et al. 2016. Understanding the Applicability and Economic Viability of Refracturing Horizontal Wells in Unconventional Plays. Presented at the SPE Hydraulic Fracturing Technology Conference, The Woodlands, Texas, USA, February 9–11, 2016, , https://doi.org/10.2118/179113-MS.

Lindsay, S. D., McNeil, F., Sackash, M. J. et al. 2011. Use of Salt-Tolerant Friction Reducer for Coiled-Tubing Applications in Unconventional Shale Formations. Presented at the SPE/ICoTA Coiled Tubing & Well Intervention Conference and Exhibition, The Woodlands, Texas, USA, April 5–6. https://doi.org/10.2118/142064-MS.

Maxwell, Shawn. 2014. *Microseismic imaging of hydraulic fracturing: Improved engineering of unconventional shale reservoirs*: Society of Exploration Geophysicists.

Mayerhofer, M.J. J., Lolon, E.P. P., Warpinski, N.R. R. et al. 2010. What Is Stimulated Reservoir Volume?. *SPE Prod & Oper* **25** (01): 89-98. https://doi.org/10.2118/119890-PA.

Montgomery, C. 2013. Fracturing Fluid Components. Presented at the ISRM International Conference for Effective and Sustainable Hydraulic Fracturing, Brisbane, Australia, May 20–22, 2013.

Pancharoen, Monrawee. 2009. Physical properties of associative polymer solutions. *Master of Science Thesis, Stanford: Department Of Energy Resources Engineering of Stanford University*.

Panja, P. and Deo, M. 2016. Factors that control condensate production from shales: surrogate reservoir models and uncertainty analysis. *SPE Reservoir Evaluation & Engineering* **19** (01): 130-141. https://doi.org/10.1504/IJOGCT.2016.078033

Panja, Palash, Conner, Tyler, and Deo, Milind. 2016. Factors controlling production in hydraulically fractured low permeability oil reservoirs. *International Journal of Oil, Gas and Coal Technology* **13** (1): 1-18.

Peña-Icart, M., Tagle, M. E. V., Alonso-Hernández, C. et al. 2011. Comparative Study of Digestion Methods EPA 3050B (HNO3–H2O2–HCl) and ISO 11466.3 (Aqua Regia) for CU, Ni and Pb Contamination Assessment in Marine Sediments. Marine environmental research 72(1-2): 60-66. https://doi.org/10.1016/j.marenvres.2011.05.005.

Portas, R. and Slatt, R. 2016. Understanding of natural fractures in the Woodford shale to improve hydrocarbon production. Presented at the International Conference and Exhibition, Barcelona, Spain, 3-6 April 2016356-356.

Seright, R. S., Campbell,A., and Mozley, P. 2009. Stability of Partially Hydrolyzed Polyacrylamides at Elevated Temperatures in the Absence of Divalent Cations. Presented at SPE International Symposium on Oilfield Chemistry, The Woodlands. Texas, 20-22 April. SPE-121460-MS. https://doi.org/10.2118/121460-MS.

Sisk, C., Diaz, E., Walls, J., et al. 2010. 3D Visualization and Classification of Pore Structure and Pore Filling in Gas Shales. Presented at the SPE Annual

Technical Conference and Exhibition, Florence, Italy, 19-22 September. SPE-134582-MS. https://doi.org/10.2118/134582-MS.

Slatt, R., McCullough, B., Molinares-Blanco, C. et al. 2016. Paleotopographic and Depositional Environmental Control on "Sweet Spot" Locations in Some Unconventional Resource Shales. Presented at the International Conference and Exhibition, Melbourne, Australia 13-16 September. https://doi.org/10.1190/ice2015-2197869.

Smith, Michael Berry and Montgomery, Carl. 2015. *Hydraulic fracturing*: Crc Press.

Sonnenberg, S. A. 2015. Keys to Production, Three Forks Formation, Williston Basin. Presented at the SPE/AAPG/SEG Unconventional Resources Technology Conference, San Antonio, Texas, USA, July 20–22, https://doi.org/10.15530/URTEC-2015-2148989.

Tessier, A., Campbell, P. G. C. and Bisson, M. 1979. Sequential Extraction Procedure for the Speciation of Particulate Trace Metals. *Analytical Chemistry* **51**(7): 844–851. 10.1021/ac50043a017.

Texans, North. 2016. An Energy Revolution: 35 Years of Fracking in the Barnett Shale.

Veazey, Matthew V. 2019. *Permian Drilling Record Reported*.

Vermylen, J. P. and Zoback, M. D. 2011. Hydraulic Fracturing, Microseismic Magnitudes, and Stress Evolution in the Barnett Shale, Texas, USA. Presented at the SPE Hydraulic Fracturing Technology Conference, The

Woodlands, Texas, USA, January 24–26, 2011, , https://doi.org/10.2118/140507-MS.

Walton, I. and McLennan, J. 2013. The Role of Natural Fractures in Shale Gas Production. Presented at the ISRM International Conference for Effective and Sustainable Hydraulic Fracturing, Brisbane, Australia, May 20–22, 2013.

Warpinski, N.R., Mayerhofer, M.J., Vincent, M.C. et al. 2009. Stimulating Unconventional Reservoirs: Maximizing Network Growth While Optimizing Fracture Conductivity. *J Can Pet Technol* **48** (10): 39-51. https://doi.org/10.2118/114173-PA.

Weddle, P., Griffin, L., and Pearson, C. M. 2017. Mining the Bakken: Driving Cluster Efficiency Higher Using Particulate Diverters. Presented at the SPE Hydraulic Fracturing Technology Conference and Exhibition, The Woodlands, Texas, USA, January 24–26, https://doi.org/10.2118/184828-MS.

Woodroof, R. A. and Anderson, R. W. 1977. Synthetic Polymer Friction Reducers Can Cause Formation Damage. Presented at the SPE Annual Fall Technical Conference and Exhibition, Denver, Colorado, 9-12 October. SPE-6812-MS. https://doi.org/10.2118/6812-MS.

Wu, J Jim, Yu, Weichu, Ding, Fei et al. 2017. A Breaker-Free, Non-Damaging Friction Reducer for AllBrine Field Conditions. *Journal of Nanoscience and Nanotechnology* **17** (9): 6919-6925.

Wu, Jun Jim. 2010. *Using dispersion polymers with nonionic characteristics and formulations to reduce friction*, Google Patents (Reprint).

Zoback, M. D., Kohli, A., Das, I. et al. 2012. The Importance of Slow Slip on Faults During Hydraulic Fracturing Stimulation of Shale Gas Reservoirs. Presented at the SPE Americas Unconventional Resources Conference, Pittsburgh, Pennsylvania USA, June 5–7, https://doi.org/10.2118/155476-MS.

Zoback, Mark D. 2010. *Reservoir geomechanics*: Cambridge University Press.